Cell Reports

Evolution of the ribbon-like organization of the Golgi apparatus in animal cells

Graphical abstract

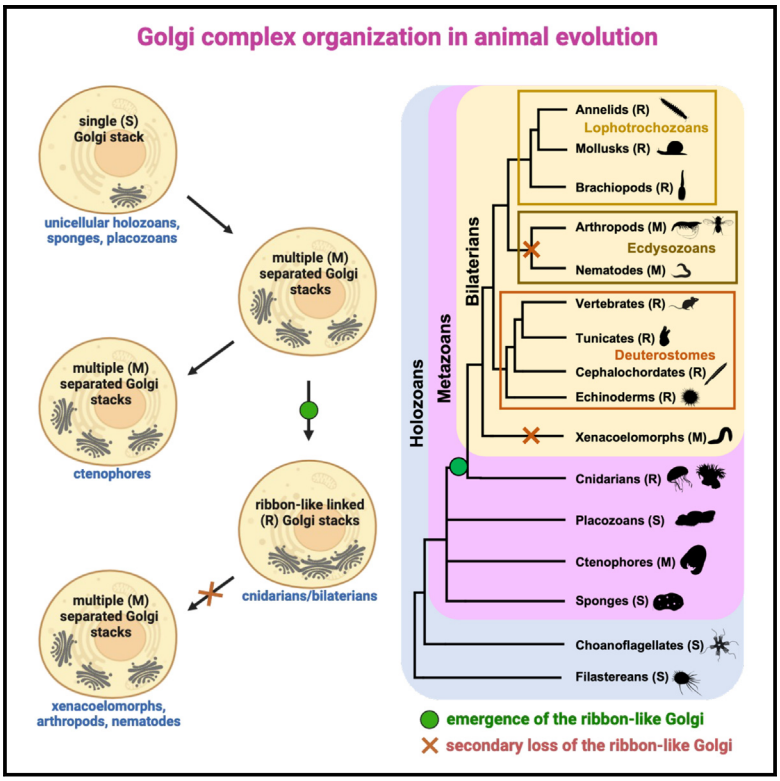

Highlights

- The cells of several animal taxa have a ribbon-like Golgi configuration
- Ribbon-like Golgi emergence may be explained by the evolution of a GRASP/golgin complex
- Formation of the ribbon-like Golgi in early embryos suggests its role in development

Authors

Giovanna Benvenuto, Serena Leone, Emanuele Astoricchio, ..., Salvatore D'Aniello, Maria Ina Arnone, Francesco Ferraro

Correspondence

francesco.ferraro@szn.it

In brief

Benvenuto et al. challenge the current consensus by revealing the pre-vertebrate origin of ribbon-like Golgi architecture and suggest a molecular basis for its evolution supported by AlphaFold modeling. Observing its formation early in embryogenesis, the authors also propose that the ribbon-like Golgi configuration plays a role in development.

Benvenuto et al., 2024, Cell Reports ■■, 113791
■■, 2024
https://doi.org/10.1016/j.celrep.2024.113791

Please cite this article in press as: Benvenuto et al., Evolution of the ribbon-like organization of the Golgi apparatus in animal cells, Cell Reports (2024), https://doi.org/10.1016/j.celrep.2024.113791

Cell Reports

CellPress
OPEN ACCESS

Report

Evolution of the ribbon-like organization of the Golgi apparatus in animal cells

Giovanna Benvenuto,[1,14] Serena Leone,[1,14] Emanuele Astoricchio,[1] Sophia Bormke,[2] Sanja Jasek,[3,4] Enrico D'Aniello,[1] Maike Kittelmann,[5] Kent McDonald,[6] Volker Hartenstein,[7] Valentina Baena,[8] Héctor Escrivà,[9] Stephanie Bertrand,[9] Bernd Schierwater,[10] Pawel Burkhardt,[11] Iñaki Ruiz-Trillo,[12,13] Gáspár Jékely,[3,4] Jack Ullrich-Lüter,[2] Carsten Lüter,[2] Salvatore D'Aniello,[1] Maria Ina Arnone,[1] and Francesco Ferraro[1,15,*]

[1]Department of Biology and Evolution of Marine Organisms, Stazione Zoologica Anton Dohrn (SZN), Naples, Italy
[2]Museum für Naturkunde, Berlin, Germany
[3]Living Systems Institute, University of Exeter, Exeter, UK
[4]Heidelberg University, Centre for Organismal Studies (COS), Heidelberg, Germany
[5]Department of Biological and Medical Sciences, Oxford Brookes University, Oxford, UK
[6]Electron Microscope Lab, University of California Berkeley, Berkeley, CA, USA
[7]Department of Molecular, Cell and Developmental Biology, University of California, Los Angeles, Los Angeles, CA, USA
[8]Department of Cell Biology, UConn Health, Farmington, CT, USA
[9]Sorbonne Université, CNRS, Biologie Intégrative des Organismes Marins, BIOM, Banyuls-sur-Mer, France
[10]Institute of Ecology and Evolution, Hannover University of Veterinary Medicine Foundation, Hannover, Germany
[11]Michael Sars Centre, University of Bergen, Bergen, Norway
[12]Institut de Biologia Evolutiva (CSIC-Universitat Pompeu Fabra), Passeig Marítim de la Barceloneta, Barcelona, Spain
[13]ICREA, Barcelona, Spain
[14]These authors contributed equally
[15]Lead contact
*Correspondence: francesco.ferraro@szn.it
https://doi.org/10.1016/j.celrep.2024.113791

SUMMARY

The "ribbon," a structural arrangement in which Golgi stacks connect to each other, is considered to be restricted to vertebrate cells. Although ribbon disruption is linked to various human pathologies, its functional role in cellular processes remains unclear. In this study, we investigate the evolutionary origin of the Golgi ribbon. We observe a ribbon-like architecture in the cells of several metazoan taxa suggesting its early emergence in animal evolution predating the appearance of vertebrates. Supported by AlphaFold2 modeling, we propose that the evolution of Golgi reassembly and stacking protein (GRASP) binding by golgin tethers may have driven the joining of Golgi stacks resulting in the ribbon-like configuration. Additionally, we find that Golgi ribbon assembly is a shared developmental feature of deuterostomes, implying a role in embryogenesis. Overall, our study points to the functional significance of the Golgi ribbon beyond vertebrates and underscores the need for further investigations to unravel its elusive biological roles.

INTRODUCTION

Sitting at the center of the exocytic pathway, the Golgi apparatus is involved in the processing and sorting of secretory cargoes. This biosynthetic function remains the most actively investigated,[1,2] but recent evidence indicate that the Golgi is also involved in secretion-independent cellular processes, such as stress sensing and signaling, apoptosis, autophagy, proteostasis, and innate immunity.[3–10] The Golgi's structural unit is the stack, formed by a pile of flat membrane saccules, known as cisternae. Across eukaryotes, the Golgi occurs as a single- or multi-copy organelle, depending on the number of stacks per cell. In animals, when present as multi-copy organelle, the Golgi is observed in two configurations: stacks either remain separate or link to each other into a single centralized structure that was first described as "ribbon-like" by Camillo Golgi.[11] The current consensus is that the Golgi ribbon is present only in vertebrate cells. Despite having been widely investigated, for the most part in cultured mammalian cells, the biological functions of the Golgi ribbon remain obscure,[12,13] and it is unclear which selective pressures might have led to the evolution of this Golgi configuration. During mitosis, mammalian cells disassemble and reassemble the ribbon in a finely tuned process[14]; such a level of regulation suggests that the ribbon architecture must be functionally important. This conclusion is supported by the existence of several pathologies in which ribbon breakdown (Golgi "fragmentation") is a morphological phenotype, most notably neurodegenerative diseases but also cancer and viral infections.[15–19] Therefore, deciphering the roles that the Golgi ribbon plays in cellular physiology may also help us understand the pathological consequences stemming from its disruption.

In this report, through a comparative approach borrowed from evolutionary studies, we asked three questions regarding the ribbon architecture of the Golgi apparatus. (1) When did it appear

Please cite this article in press as: Benvenuto et al., Evolution of the ribbon-like organization of the Golgi apparatus in animal cells, Cell Reports (2024), https://doi.org/10.1016/j.celrep.2024.113791

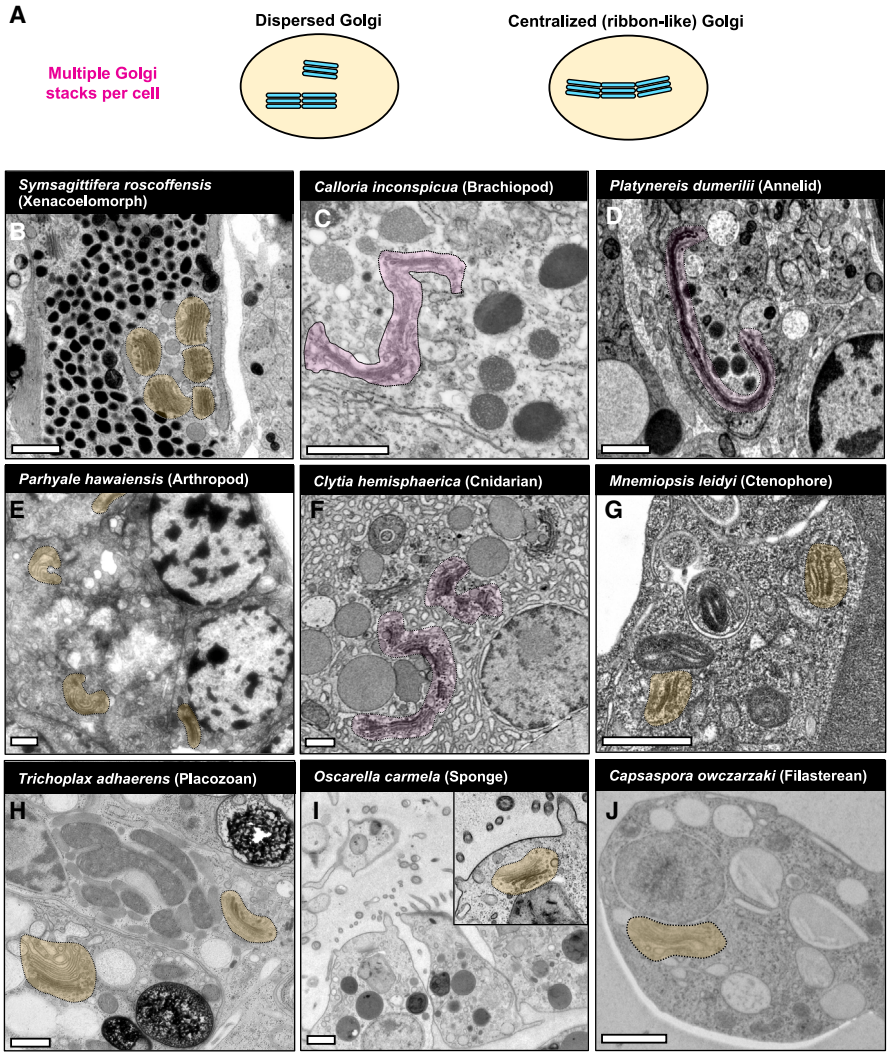

(legend on next page)

Please cite this article in press as: Benvenuto et al., Evolution of the ribbon-like organization of the Golgi apparatus in animal cells, Cell Reports (2024), https://doi.org/10.1016/j.celrep.2024.113791

during animal evolution? (2) Which molecules might have mediated this structural innovation? (3) Which biological functions does it carry out? We answer the first one and propose a testable hypothesis for the second one, and, regarding the third one, we produce experimental data that point toward development as a biological process in which the ribbon may play a functional role.

RESULTS

A ribbon-like Golgi complex is common in animals

According to the current consensus, only vertebrate cells display Golgi ribbons. Therefore, we were intrigued by morphological data showing Golgi centralization in the embryos of two sea urchin species, *Strongylocentrotus purpuratus* and *Lytechinus variegatus*,[20,21] hinting at the possibility that the ribbon organization of the Golgi might be more common than thought at present. To assess if this is the case, we surveyed the Golgi ultrastructure in representatives of several animal taxa and closely related unicellular eukaryotes, which, together, comprise the holozoan clade. We assessed Golgi morphology in animal cells from published studies and generated data from those taxa for which there was no information available in the literature. In our morphological survey, we distinguished between *bona fide* ribbon and ribbon-like architectures. In mammalian cells, the Golgi ribbon is characterized by some level of membrane continuity between cisternae of adjacent stacks, which can be detected by fluorescence recovery after photobleaching assays and electron tomography.[22,23] As our survey relied, for the most part, on electron micrographs of thin sections where membrane continuity between cisternae of juxtaposed stacks cannot be easily evaluated, we describe Golgi organizations reminiscent of the mammalian ribbon as ribbon-like. Golgi stack dimers have been observed in *Drosophila melanogaster* cells,[24] which have dispersed Golgi elements,[25] and even in mammalian cells after ribbon unlinking by microtubule depolymerization.[26] Therefore, we identified Golgi complexes as ribbon-like only when three or more closely apposed stacks were observed in electron micrographs (Figure 1A). Although the ribbon is the default Golgi architecture of mammalian cells, there are exceptions. Differentiated cell types such as muscle cells, acid-secreting gastric cells, and spinal ganglion neurons display Golgi complexes made by separated stacks.[27–29] In megakaryocytes, the Golgi ribbon is disassembled into individual stacks, which are packaged into nascent platelets.[30] These examples indicate that the Golgi configuration can vary depending on the cell type; therefore, wherever possible, we inspected several tissues of the organisms under consideration.

We first looked at bilaterians. In the cells of the marine worm *Symsagittifera roscoffensis* (xenacoelomorph), separated stacks were observed (data not shown). Interestingly, some of its secretory cells displayed closely apposed, though clearly distinct, Golgi stacks: an intermediate organization between separated Golgi elements and a ribbon-like organization (Figures 1B and S1A). Ribbon-like Golgis were found in epidermal cells of the three-lobed larva of the brachiopod *Calloria inconspicua* and in several cell types of the marine annelid *Platynereis dumerilii* (Figures 1C, 1D, and S1B; Video S1). As Ramón y Cajal reported Golgi complexes that look unmistakably ribbon-like in neurons and epithelial cells of the common earthworm,[31] we conclude that this Golgi organization is common among annelids. In mollusks, a centralized Golgi that fragments at mitosis was observed in spermatocytes of the snail *Paludina vivipara* more than a century ago,[32] and inspection of images of other species (*Helix pomatia*[33] and *Helix aspersa*[34]) reveals Golgi complexes with a ribbon-like organization. Cells of the roundworm *Caenorhabditis elegans*, a nematode, and of the fruit fly *D. melanogaster*, an arthropod, two model organisms widely used in genetics and cell biology, display Golgi complexes consisting of several separated stacks.[24,25,35] To test whether Golgi stack decentralization is an arthropod feature, as opposed to *Drosophila*/insect-specific, we analyzed the ultrastructure of the crustacean *Parhyale hawaiensis*, observing separated stacks in neurons (Figure 1E) and in all other inspected cell types (data not shown). It is therefore likely that a decentralized Golgi is the typical configuration in arthropods, not just of *Drosophila* and other insects (e.g., bees, aphids, and mosquitos[36–38]). We then analyzed cnidarians: in the hydrozoan *Clytia hemisphaerica*, the secretory gland cells of the gastroderm, but not other cell types, display stacks linked into a ribbon-like structure (Figure 1F), which is also observed in phagocytic cells of another cnidarian, the actinia *Phelliactis robusta*.[39] In the ctenophore *Mnemiopsis leidyi*, epithelial and comb cells (Figures 1G and S1C), nerve net neurons, mesogleal neurons, and sensory cells (data not shown) all display separated stacks. Among other animals, we found a single Golgi

Figure 1. Golgi architecture in holozoans

The Golgi ultrastructure was analyzed in holozoan exemplars; separated and linked Golgi stacks are highlighted in ochre and magenta, respectively.

(A) Presence of three or more Golgi stacks in close contact is the criterion adopted for positive identification of the ribbon-like configuration in electron micrographs.

(B) The xenacoelomorph *Symsagittifera roscoffensis*, secretory cell.

(C) The brachiopod *Calloria inconspicua*, epidermal cell of the mantle lobe of the three-lobed larva.

(D) The annelid *Platynereis dumerilii*, glial cell of the 3-day-old larva.

(E) The crustacean *Parhyale hawaiensis*, nerve cell.

(F) The cnidarian *Clytia hemisphaerica*, gastrodermal cell.

(G) The ctenophore *Mnemiopsis leidyi*, epithelial cells.

(H) The placozoan *Tricoplax adhaerens,* non-epithelial cell.

(I) The sea sponge *Oscarella carmela*, choanocyte.

(J) The filasterean *Capsaspora owczarzaki.* Scale bars: 1 μm.

(K) Deduced evolutionary emergence of the ribbon-like Golgi organization. Ribbon-like absence in both arthropods and nematodes, which both belong to the ecdysozoan superphylum, may indicate that loss of Golgi stack linking occurred in their common ancestor.

See also Figure S1 and Video S1.

Please cite this article in press as: Benvenuto et al., Evolution of the ribbon-like organization of the Golgi apparatus in animal cells, Cell Reports (2024), https://doi.org/10.1016/j.celrep.2024.113791

stack in all cells of two placozoan species: *Trichoplax adhaerens* (Figures 1H, S1D, and S1E) and *Hoilungia hongkongensis*.[40] Like placozoans, the sea sponge *Oscarella carmela* (Figure 1I; Laundon et al.[41]) and other species (genera *Chondrosia*, *Crambe*, and *Petrosia*; data not shown) have a single Golgi stack per cell. In choanoflagellates and filastereans, which are unicellular holozoans, the Golgi is also present as a single stack per cell (Figure 1J; Laundon et al.[41] and Burkhardt et al.[42]).

Vertebrates (chordates) and echinoderms (ambulacraria) belong to the deuterostome clade of bilaterian animals. We assessed whether the Golgi ribbon is found in non-vertebrate deuterostomes, investigating the ultrastructure of a sea urchin, a tunicate, and a cephalochordate. Indeed, we find that all three species display ribbon-like Golgis (see developmental assembly of the Golgi ribbon below). Based on our survey, except for ctenophores, cells with Golgi complexes consisting of multiple stacks are observed only in cnidarians and bilaterians.

In summary, despite a relatively small sampling (Figure S1F), ribbon-like Golgi complexes are easily observed in cells of cnidarians and bilaterians and are not found outside these animal taxa. The most parsimonious explanation for our findings is that the ribbon-like Golgi likely evolved in the common ancestor of cnidarians and bilaterians and was secondarily lost in xenacoelomorphs, arthropods, and nematodes (Figure 1K). It is worth pointing out that ours represents a coarse-grained outline of the ribbon-like Golgi occurrence in animals, and future deeper sampling may identify other events of secondary loss.

Except for *P. dumerilii* and *S. purpuratus* (Figures S1B and S4E; Video S1), for which volume electron microscopy was available, the thin-section electron micrographs produced for our survey did not allow us to assess whether all the Golgi stacks in a cell are linked into a single ribbon-like organization or form multiple "mini-ribbons." Nonetheless, in those cases where we identified the ribbon-like configuration, it is clear that stack centralization is occurring.

Obviously, in species with a single-copy Golgi (such as unicellular holozoans, sponges, and placozoans), a ribbon-like Golgi cannot occur. However, the presence of multiple stacks does not seem sufficient for the assembly of the ribbon-like configuration. This is exemplified by ctenophores (Figure 1G) and, more strikingly, sponges. While sponges usually display a single Golgi stack per cell (Figure 1I; Laundon et al.[41]), in rare instances, such as the gemmule's spongocytes of *Ephydatia fluviatilis*,[43] multiple stacks are observed but remain separate. These observations surmise the existence of a dedicated machinery for Golgi stack tethering in the metazoan taxa displaying the ribbon-like configuration.

Putative molecular mediators of ribbon-like Golgi emergence

Next, we asked which molecular innovations might have driven stack tethering in cells with multi-copy Golgi complexes. If this was a single evolutionary event, as our survey seems to suggest, then the molecular effectors of stack tethering should be conserved across phyla. The Golgi ribbon mechanics has been studied mostly in mammalian cells, and among the several factors involved in its formation, the molecular tethers GRASP (Golgi reassembly and stacking protein) and the coiled-coil proteins collectively known as golgins play a central role (Figure 2A).[44–48] GRASPs comprise a highly conserved GRASP region, made of two atypical PDZ domains in tandem, and a highly variable C-terminal unstructured region (Figures S2A and S2B). GRASPs are encoded by a single gene in most eukaryotes, whereas a duplication event in jawed vertebrates gave rise to two paralogs, GRASP65 and GRASP55, with the latter being more similar to the single GRASP of most bilaterians and cnidarians (Figures S2C and S2D; Data S1A and S1B). GRASPs are involved in several cellular processes, ranging from exocytosis and Golgi enzyme localization to stress sensing, unconventional secretion, and autophagy.[49–54] Capable of self-interaction,[55] GRASPs were originally identified as mediators of cisternal adhesion within the Golgi stack[55–57]; recent studies indicate that they are essential to Golgi stack tethering and ribbon formation.[47,48]

Mammalian GRASP55 and GRASP65 are recruited to Golgi membranes by myristoylation of the glycine in position 2[56,58] and by interaction with golgins (Figure 2A).[59,60] Such dual anchoring is required for ribbon formation because it spatially orients GRASPs, allowing their homo-dimerization/oligomerization in *trans*, thus tethering membranes of distinct Golgi stacks.[61–63] Golgins mediate vesicular traffic specificity,[64,65] and their knockdown results in secretory defects and ribbon unlinking into constituent stacks.[45] In mammals, the golgins GM130 and Golgin-45, respectively, interact with GRASP65 and GRASP55 (Figure 2A),[56,60] and knockdown of either leads to Golgi ribbon unlinking into separate stacks.[60,66] As the N-terminal glycine of GRASPs is conserved across holozoans (Data S1A), and therefore very likely also its myristoylation, we reasoned that evolution of the second anchor point for GRASPs, through golgin binding, may have led to the emergence of Golgi stack tethering and therefore the appearance of the ribbon-like Golgi organization (Figure 2B).

The X-ray structures of mammalian GRASP55 and GRASP65 in complex, respectively, with the C termini of Golgin-45 and GM130 have been solved, revealing the golgins' residues necessary for GRASP domain binding.[67,68] The very terminal residues of Golgin-45 and GM130 form PDZ-binding motifs, which interact with the PDZ1 domains of GRASP55 and GRASP65, respectively (Figure S2E).[67,68] Besides that, the interactions observed in the two complexes differ: two cysteines of Golgin-45 interact with a cysteine and a histidine of GRASP55, forming an atypical zinc finger (Figure S2E).[67] Instead, a peculiar "boot-like" conformation is adopted by GM130 in complex with GRASP65, with additional interactions established through hydrophobic residues with the groove between the two PDZ domains (Figure S2E).[68] Mutations in these regions of the two golgins abolish binding to the GRASP domains.[67,68]

The *Golgin-45* and *GM130* genes are holozoan innovations.[69] Accordingly, we identified their homologs in animals and their closest unicellular relatives. We also found that the *Golgin-45* gene was lost in choanoflagellates and, among metazoans, in most xenacoelomorphs (Data S2A), which do not display a ribbon-like Golgi (Figures 1B and S1A). By contrast, GM130 is present in all the holozoan species investigated (Data S2B). To assess conservation of the motifs required for GRASP binding, we aligned the C-terminal sequences of the holozoan homologs of the two golgins. Overall, we found a high level of conservation

Please cite this article in press as: Benvenuto et al., Evolution of the ribbon-like organization of the Golgi apparatus in animal cells, Cell Reports (2024), https://doi.org/10.1016/j.celrep.2024.113791

CellPress
OPEN ACCESS

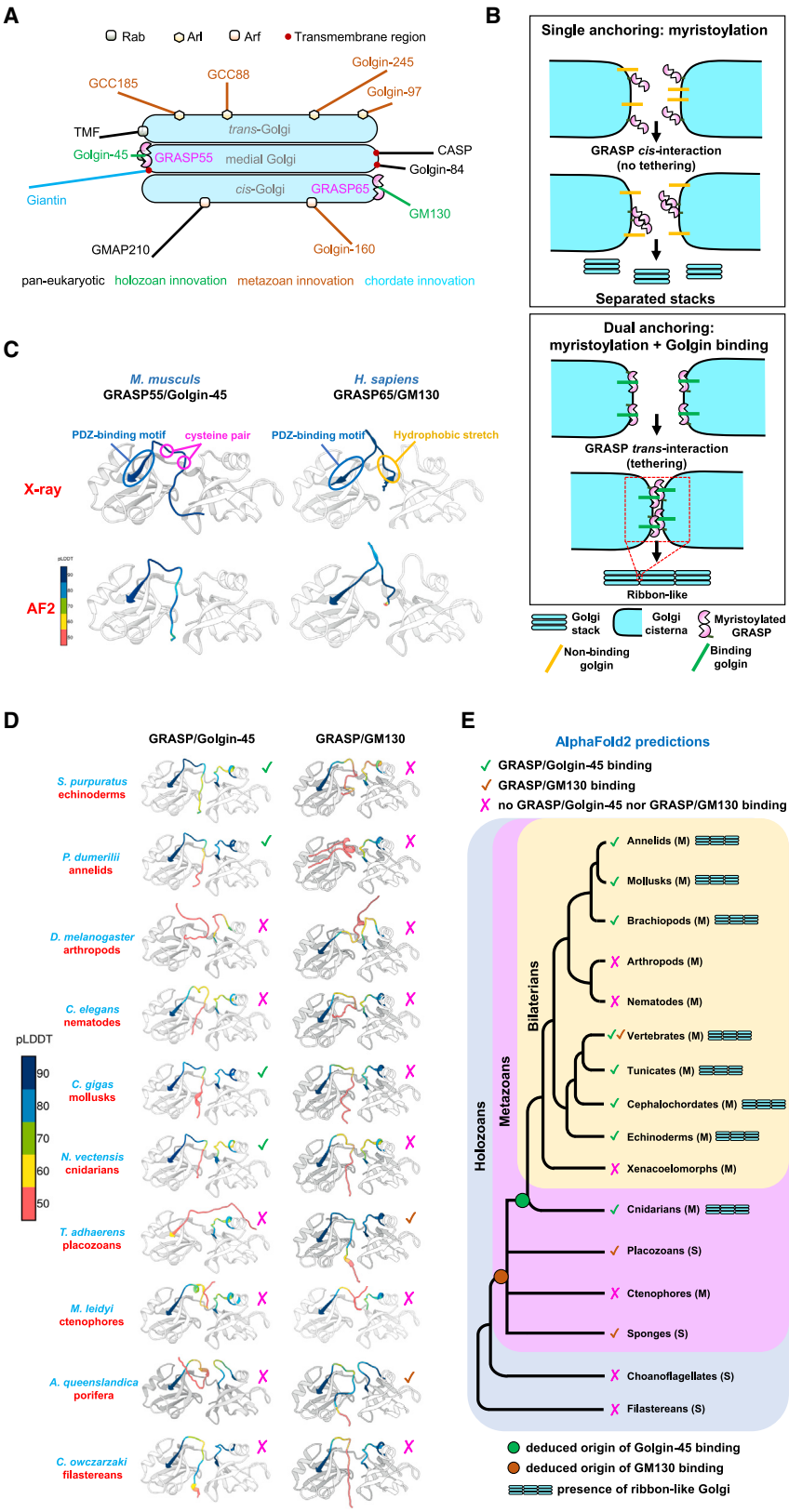

Figure 2. Putative molecular mediators of the ribbon-like Golgi emergence

(A) The Golgi localized molecular tethers Golgins and GRASPs. Golgins localize to Golgi membranes by a transmembrane region or through recruitment by small GTPases of the Rab, Arf, and Arl families. Golgin and GRASP localization within the stack, Golgin sizes (human homologs, bar length), and evolutionary emergence are indicated.

(B) Dual anchoring of mammalian GRASPs on Golgi membranes is required for self-interaction in *trans* and stack tethering. As GRASP myristoylation is ancestral (see main text and Data S1), its dual anchoring to the Golgi membrane might have originated from the evolution of binding by golgins, leading to the emergence of stack linking and ribbon formation.

(C) X-ray structures and AlphaFold2 (AF2) models of the mammalian GRASP55/Golgin-45 and GRASP65/GM130 complexes. Motifs crucial for interaction of the golgins' C termini to the respective GRASP domains are indicated.

(D) AF2 models of holozoan GRASPs in complex with the C termini of their conspecific Golgin-45 and GM130 homologs. Presence and absence of deduced binding are indicated by the symbols ✓ (green for Golgin-45, brown for GM130) and ✗, respectively.

(E) Evolutionary origin of GRASP binding by the C termini of Golgin-45 and GM130 (color coded with the same symbols used in D) as deduced by AF2 models. Single- and multi-copy Golgi are indicated by (S) and (M), respectively. Presence of the ribbon-like Golgi in metazoan clades is indicated by the cartoon.

See also Figures S2 and S3 and Data S1 and S2.

Please cite this article in press as: Benvenuto et al., Evolution of the ribbon-like organization of the Golgi apparatus in animal cells, Cell Reports (2024), https://doi.org/10.1016/j.celrep.2024.113791

of the motifs in Golgin-45 homologs (Figure S2F) and, interestingly, the occurrence of Golgin-45-like motifs in several of the non-vertebrate GM130 homologs (Figure S2G; method details). These observations are compatible with early evolution in the metazoan lineage of GRASP binding by Golgin-45 and GM130.

To further assess the possibility of GRASP binding by Golgin-45 and GM130 homologs, we took advantage of protein complex structure prediction by AlphaFold2. Compared to simple sequence analysis, AlphaFold2 accounts for the collective contribution of each amino acid of the golgin and of the apposed GRASP, thus yielding more accurate predictions.[70,71] We initially validated the approach by performing untemplated predictions of mammalian GRASP55/Golgin-45 and GRASP65/GM130 complexes, which were modeled with high confidence (pLDDT $\geq$ 80; for the definition of pLLDT, see method details) and appeared highly similar to the crystal structures (Figure 2C). Then, complexes with point mutants of Golgin-45 and GM130 experimentally shown to abolish binding[67,68] were modeled, and AlphaFold2 produced results that paralleled the biochemical data in the case of Golgin-45 mutants (i.e., lower-confidence models, pLDDT < 70), though not in the case of GM130 mutants (Figures S3A–S3D; but see considerations on GM130 mutants in the method details). In mammalian cells, GRASP55/Golgin-45 and GRASP65/GM130 interactions are specific. However, co-immunoprecipitation experiments show that GM130 can also interact with GRASP55, but Golgin-45 cannot interact with GRASP65.[60] Challenged with these cross-interactions, AlphaFold2 modeled the GRASP55/GM130 complex, but not the GRASP65/Golgin-45 one, with pLDDT >70 and a conformation similar to the X-ray structure (Figures S3E, S3F, and 2C). Based on the success of these validation tests, AlphaFold2 seems to provide reliable structural predictions in most cases. We therefore employed it to infer conspecific GRASP/golgin interactions in extant holozoan species.[70–72] For each protein pair analyzed, we considered binding to occur when, in their AlphaFold2 model, the regions mediating interaction of golgins to GRASPs in the mammalian complexes (the PDZ-binding motifs, the cysteine pair, and the hydrophobic stretch; Figure S2E) displayed conformations similar to those in the reference X-ray structures and were modeled with pLDDT scores $\geq$70[73] (Figures 2C and S2E).

Regarding the GRASP/Golgin-45 complex, interaction was predicted in all bilaterians and cnidarians except for the arthropods *D. melanogaster* (Figure 2D) and *P. hawaiensis* (data not shown), the nematode *C. elegans* (Figure 2D), and *Hofstenia miamia*, the only xenacoelomorph species in which the *Golgin-45* gene was found (data not shown). No binding was predicted in placozoans, ctenophores, porifera, and unicellular filastereans (Figure 2D). With respect to GM130, as it could be anticipated from the amino acid sequences (Figure S2G), AlphaFold2 models of the vertebrate homologs predicted binding to the conspecific GRASP65 paralogs with high pLDDT and conformations very similar to those of the human protein (Figures S3G and S3H). However, in several non-vertebrate holozoans the GM130 C terminus sequence resembles that of Golgin-45, with a cysteine pair and the PDZ-binding motif, suggesting that in these species GM130 might interact with GRASP in a Golgin-45-like fashion. Indeed, GRASP/GM130 AlphaFold2 models predicted interaction with a conformation similar to that of the GRASP/Golgin-45 complex for the proteins from sponges and placozoans, although not for the other species investigated (Figure 2D). As AlphaFold2 relies on the generation of a multiple sequence alignment,[70,72,74] divergent sequences might result in unreliable models, characterized by lower pLDDT scores. To assess how this factor could influence the results of our predictions, we modeled the GRASP/golgin complexes of the fast-evolving species *Ciona robusta*, which displays ribbon-like Golgi complexes (see developmental assembly of the Golgi ribbon below) and whose single GRASP's sequence is divergent (Figure S2D). AlphaFold2 predicted the binding of Golgin-45 but not of GM130 to GRASP (Figures S3I and S3J). Interestingly, the *C. robusta* GM130 homolog is missing one of the two putative zinc finger-forming cysteines (Figure S2G; method details), which might explain the AlphaFold2 prediction.

In our analysis, we assumed that the interaction between golgins and GRASPs is an evolutionarily conserved feature. In this framework, the models generated by AlphaFold2 provide support for the appearance of GRASP binding by GM130 and Golgin-45 during the evolutionary history of metazoans. Specifically, the models indicate that GRASP binding by GM130 likely evolved in the common ancestor of metazoans but was later lost in most phyla. On the other hand, binding by Golgin-45 appears to have evolved in the common ancestor of cnidarians and bilaterians, with subsequent losses in arthropods, nematodes, and xenacoelomorphs (Figure 2E). Interestingly, as GRASP paralogs emerged in vertebrates, GM130 and Golgin-45 diverged in their C-terminal sequences, resulting in distinct binding conformations (Figures 2C, S2G, S3G, and S3H).

In summary, the AlphaFold2 models align with our hypothesis that dual anchoring of GRASP to Golgi membranes by golgins could have driven Golgi stack tethering and the emergence of the ribbon-like Golgi (Figure 2E). This innovation could only occur in an ancestral metazoan with a multi-copy Golgi, which, based on our morphological survey, is likely to correspond to the cnidarian/bilaterian common ancestor (Figures 1 and S1). However, the presence of multi-stack Golgi complexes in extant ctenophores (Figure 1G) raises the possibility that a ribbon-like configuration, mediated by the GRASP/GM130 interaction, may have been originally present in this phylum and subsequently lost during evolution.

Developmental assembly of the Golgi ribbon

As published morphological data were indicative of Golgi centralization in developing sea urchins,[20,21] we analyzed Golgi dynamics in the embryo of the sea urchin species *Paracentrotus lividus*. Time course analysis of a fluorescent Golgi reporter showed that early in development, throughout the cleavage stage, the Golgi is present as separate elements, which then cluster into centralized structures before hatching of the blastula (Figures 3A, S4A, and S4B). Golgi clustering is rapid: within 1 h, Golgi elements increase 10-fold in size, while their number decreases 3-fold (Figures 3B and 3C; Video S2). Afterward, centralized Golgi complexes are observed in all cells of the embryo and at all developmental stages up to the planktonic pluteus larva (Figures 3A and S4C). Confocal imaging at higher magnification of post-clustering stages showed a morphology strongly reminiscent of the Golgi ribbon as observed in mammalian cells

Please cite this article in press as: Benvenuto et al., Evolution of the ribbon-like organization of the Golgi apparatus in animal cells, Cell Reports (2024), https://doi.org/10.1016/j.celrep.2024.113791

CellPress
OPEN ACCESS

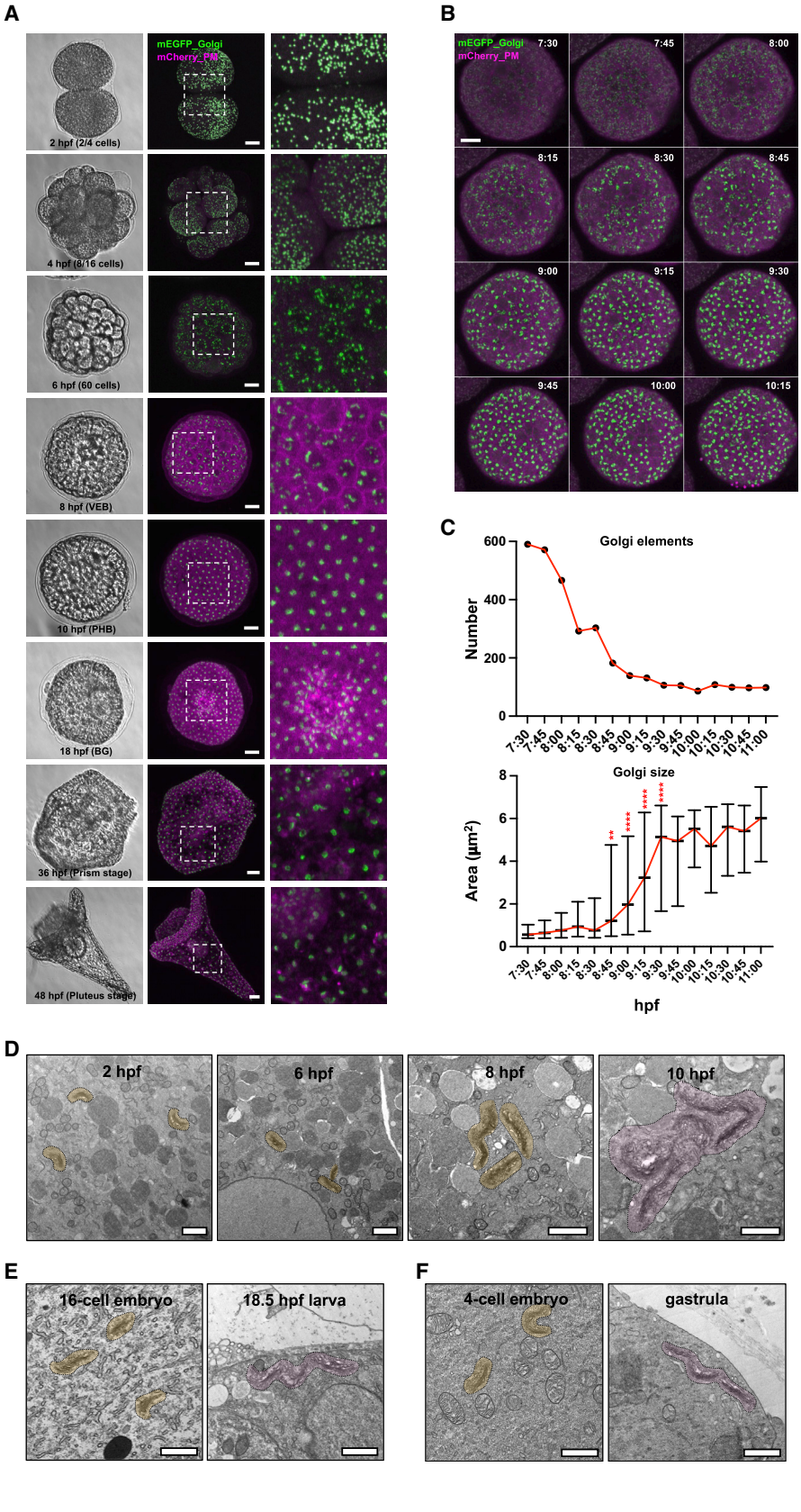

(legend on next page)

Please cite this article in press as: Benvenuto et al., Evolution of the ribbon-like organization of the Golgi apparatus in animal cells, Cell Reports (2024), https://doi.org/10.1016/j.celrep.2024.113791

(Figure S4D). At the ultrastructural level, the arrangement of the sea urchin Golgi elements recapitulated confocal microscopy observations. Separated stacks cluster and finally establish connections with each other during early development, confirming that sea urchins centralize their Golgi apparatus into a ribbon-like architecture (Figure 3D). Centralized Golgi complexes were previously observed by light microscopy in the gastrula and prism stages of *S. purpuratus*.[20] Indeed, we also observed ribbon-like Golgi complexes in the pluteus larva of this sea urchin species (Figure S4E). Like the ribbon of mammalian cells, the sea urchin's centralized Golgi undergoes disassembly/reassembly cycles during mitosis (Figure S4F), and its maintenance requires an intact microtubule network (Figures S4G and S4H).[12,14,75,76] All these characteristics strongly indicate that the centralized Golgi complexes of sea urchin cells are *bona fide* ribbons.

As echinoderm representatives, sea urchins form part of the sister group to all chordates, including vertebrates. Therefore, the mechanisms mediating formation of the Golgi ribbon and its developmental timing might be conserved across the deuterostome clade. Indeed, we observed developmental Golgi stack clustering and ribbon-like formation in the cells of two non-vertebrate chordates, the sea squirt *C. robusta* (tunicate) and the lancelet *Branchiostoma lanceolatum* (cephalochordate) (Figures 3E and 3F). Notably, Golgi centralization is also observed in mouse embryos during the pre-implantation stage,[77] indicating that developmental ribbon assembly is a conserved feature across deuterostomes. The time of ribbon formation in the sea urchin embryo is significant. In the pre-hatching blastula, although the embryo's cells are morphologically undistinguishable, they differentially express cell-fate-determining transcription factors.[78] The developmental switch from separated Golgi stacks to the ribbon-like configuration might, therefore, be functional to the initial stages of embryogenesis.

DISCUSSION

Although the functions played by the ribbon remain unaddressed, indirect evidence suggest that this Golgi configuration must be important to cellular physiology. Firstly, the mammalian ribbon disassembles and reassembles during mitosis in proliferating cells; this process involves a finely timed regulation,[12,14] which is unlikely to have evolved to preserve a cellular structure with no biological role. Secondly, Golgi fragmentation, which involves different modalities of ribbon disruption,[79] is a morphological phenotype of several human pathologies, among which are neurodegenerative diseases. Golgi fragmentation precedes phenotypic manifestations in animal models of amyotrophic lateral sclerosis.[15] In cellular models of Alzheimer's disease, Golgi fragmentation promotes Aβ peptide production,[16] and it is one of the earliest morphological phenotypes detected in glutamatergic neurons differentiated from induced pluripotent stem cells (iPSCs) that carry familial Alzheimer's disease mutations.[19] From these observations, it follows that identification of the biological functions of the Golgi ribbon would not only advance our knowledge of cellular physiology but also help to understand the pathological implications of this structure's disruption. By adopting a comparative perspective that places Golgi architecture in an evolutionary context, here, we outline the origins of the ribbon-like organization, propose putative molecular drivers of its emergence, and describe its developmentally regulated formation, which may signal its function in embryogenesis.

Previous to the present study, the ribbon organization of the Golgi apparatus was thought to be unique to vertebrates. The lack of a centralized Golgi in the cells of *D. melanogaster* and *C. elegans*, two invertebrates widely used in cell biology, may have contributed to cement this view, despite the ribbon-like Golgi organization, although not described as such, could be observed in a few studies on invertebrates.[20,21,31–34,39] Building on this sparse evidence, we further sampled metazoan taxa and found that the ribbon-like centralization of Golgi stacks is likely to be a newly evolved character of the ancestor of cnidarians and bilaterians (Figure 1K). Evolutionary conservation of the ribbon-like Golgi configuration in several animal phyla strongly indicates that it must play important functions in their cellular processes. It also begs the question of how the cells of xenacoelomorphs and ecdysozoans adapted to its secondary loss. Comparative analysis of cellular processes in animals with the ribbon-like Golgi and in those that lost it may provide clues regarding the functions this structure is involved in.

Our conclusion that the ribbon-like appearance was a single evolutionary event implies conservation of its core molecular machinery. Emergence of the ribbon-like architecture must depend on the evolution of Golgi stack tethering. Based on mechanistic evidence from mammalian cells, we focused on known Golgi tethering factors. GRASP was part of the molecular toolkit of the last eukaryotic common ancestor.[69] Biophysical evidence indicates that its ability to form dimers and oligomers is ancestral,[55,80] and functional data suggest that a conserved function of GRASPs is that of a "multi-tasking" membrane tether[52] in cellular stress responses.[49–51] Bootstrapping on its self-interacting and tethering capabilities, and in the context of cells with multiple Golgi stacks, evolution of a second GRASP anchoring point on Golgi membranes through golgin binding

Figure 3. Developmental assembly of the Golgi ribbon

(A) Embryos of the sea urchin *Paracentrotus lividus* expressing Golgi and plasma membrane (PM) fluorescent reporters were imaged at the indicated stages (hpf, hours postfertilization; VEB, very early blastula; PHB, pre-hatching blastula; BG, blastopore gastrula) by bright-field and confocal microscopy (maximum intensity projections are shown); scale bars: 20 μm.

(B) Time-lapse confocal microscopy (maximum intensity projections) of an embryo microinjected as described in (A) and imaged at the indicated times (hpf); scale bar: 20 μm.

(C) Number and size (median and interquartile range are shown) of Golgi objects in the embryo shown in (B) were measured; $^{**}p < 0.01$ and $^{****}p < 0.0001$; Mann-Whitney test, compared to 8.5 hpf.

(D–F) Golgi ultrastructure of (D) *Paracentrotus lividus*, (E) *Ciona robusta*, and (F) *Branchiostoma lanceolatum* embryos at the indicated developmental stages; Golgi complexes are outlined (isolated stacks in ochre; linked stacks in magenta); scale bars: 1 μm.

See also Figure S4 and Video S2.

Please cite this article in press as: Benvenuto et al., Evolution of the ribbon-like organization of the Golgi apparatus in animal cells, Cell Reports (2024), https://doi.org/10.1016/j.celrep.2024.113791

may have therefore driven ribbon-like emergence (Figure 2B). This hypothesis invokes a central role for the GRASP/golgins interaction in the evolution and conservation of the mechanism of formation of the ribbon-like Golgi. We investigated this possibility by predicting binding of golgins to GRASPs using AlphaFold2. Based on the models of GRASP/golgin complexes in present-day species, we deduce that GRASP binding by Golgin-45 evolved in the common ancestor of cnidarians and bilaterians, in correspondence with the emergence of the ribbon-like organization. Modeling suggests that the GRASP/Golgin-45 complex is highly conserved and secondarily lost in species documented to lack the ribbon-like Golgi organization (Figure 2E). In addition, the models point to the evolution of binding between GM130 and GRASP in the common ancestor of metazoans, followed by multiple secondary losses (Figure 2E). This scenario may reflect the fact that these ancestral metazoans were likely to have a single-copy Golgi, and therefore selective pressure for GRASP dual anchoring by GM130 could have been absent. On the other hand, the appearance of metazoans displaying multiple stacks per cell and the emergence of the ribbon-like Golgi may have led to selective pressure for the conservation of the GRASP/Golgin-45 complex. In this framework, GM130 contribution to stack tethering in non-vertebrate animals appears to be unnecessary or at most redundant. In summary, AlphaFold2 modeling provides support for our hypothesis that evolution of GRASP binding by golgins may have driven the emergence of the ribbon-like Golgi architecture.

In eukaryotes, complex multi-cellularity evolved several times,[81] but non-animal multi-cellular organisms, such as plants and fungi, display multiple separated Golgi stacks.[82,83] Golgi centralization may thus indicate an evolutionary trajectory with functional requirements specific to cnidarians/bilaterians. The question thus arises as to which functions the ribbon-like Golgi organization evolved to carry out. If the ribbon, as believed until now, was a configuration restricted to vertebrates, then its functions might be struck off as specific to this animal lineage. Our findings imply otherwise; while in the 600 million years since its appearance, the ribbon-like Golgi may have accrued lineage-specific functions, at least some of the biological processes it attends to are likely to be common to all cnidarians/bilaterians. The observation that the ribbon is formed early in embryogenesis (this report and Kiyonari et al.[77]) may indicate that its first function, in the context of the whole organism, is linked to development. This would explain why some differentiated mammalian cells can forgo Golgi ribbons.[27–29] Of note, mammalian embryonic stem cell lines often display unlinked Golgi stacks, and their differentiation is accompanied by ribbon formation.[84,85] iPSCs seem to have unlinked Golgi stacks as well,[86] and, remarkably, drugs used to reprogram differentiated cells into iPSCs (e.g., GSK3 and HDAC inhibitors)[87] induce ribbon disruption in mammalian cells lines.[88] These observations suggest a correlation between Golgi architecture and the pluripotent/differentiated state of cells. Ribbon formation could therefore have a function in cell differentiation. From an evolutionary point of view, it is intriguing to speculate that this may also have been the primordial role of the ribbon-like Golgi. In this hypothetical scenario, the developmental processes of xenacoelomorphs, arthropods, and nematodes must have adapted to dispense with the ribbon-like Golgi altogether. We anticipate that comparative approaches employing newly introduced experimental invertebrates[89–91] and other established vertebrate and invertebrate models will be instrumental to unravel the range of functions that the ribbon-like Golgi plays in animal cells.

In conclusion, Golgi centralization into a ribbon-like configuration is common to several animal taxa; by the principle of parsimony, we assume that this reflects a single evolutionary event occurring in their common ancestor. Ribbon formation during early embryogenesis suggests an unexplored, and perhaps primordial, function for this Golgi architecture in development. We expect that our report will spark renewed interest in the ribbon-like configuration of the Golgi apparatus and new studies aimed at testing our hypotheses on its molecular origins and on its function in the context of development.

Limitations of the study

Despite the powerful capabilities of AlphaFold2, interaction of GRASP with conspecific golgins remains to be experimentally validated in non-vertebrates. Also, whether the binding between golgins and GRASP is itself sufficient to induce stack tethering and whether the linked Golgi stacks documented in non-vertebrates reflect the presence of *bona fide* ribbons need to be established through experiment. In other words, it needs to be established whether the golgin-dependent spatial orientation of GRASP on Golgi membranes is conducive not only to stack tethering but also to membrane continuity between cisternae of juxtaposed stacks, as observed in mammalian cells.[22,23] Mammalian GRASPs are necessary for ribbon formation and interact with tens of proteins.[48,92] Therefore, it is possible that by recruiting a network of interactors, oligomerization of correctly oriented GRASPs could provide a multivalent molecular platform that directly mediates Golgi stack tethering and indirectly coordinates the activity of several factors in the formation and maintenance of the Golgi ribbon. Future studies will put to the test our hypothesis on the structural determinants of the ribbon-like Golgi organization. To validate AlphaFold2 predictions, biochemical binding assays could be employed with GRASP/golgin pairs from species in key places in the metazoan tree. Whether GRASP/golgin interactions are sufficient to induce ribbon-like Golgi organization could be assessed by introducing heterologous GRASP/golgin pairs into cellular systems with non-functional homologs and separate Golgi stacks.

STAR★METHODS

Detailed methods are provided in the online version of this paper and include the following:

- KEY RESOURCES TABLE
- RESOURCE AVAILABILITY
  - Lead contact
  - Materials availability
  - Data and code availability
- EXPERIMENTAL MODEL AND STUDY PARTICIPANT DETAILS
  - *Paracentrotus lividus*
  - *Branchiostoma lanceolatum*

SUPPLEMENTAL INFORMATION

Supplemental information can be found online at https://doi.org/10.1016/j.celrep.2024.113791.

ACKNOWLEDGMENTS

We thank Laura Núñez Pons, Filomena Ristoratore, and Periklis Paganos (Stazione Zoologica Anton Dohrn, SZN, Naples, Italy) for providing electron micrographs of sea sponges and the sea urchin *S. purpuratus* and for helping with the anatomy of the *C. robusta* larva; Evelyn Houliston (Laboratoire de Biologie du Développement de Villefranche-sur-mer, Villefranche-sur-Mer, France) and Mark Terasaki (UConn Health, Farmington, CT, USA) for identifying the ribbon-like Golgi configuration in *C. hemisphaerica*; Elisabeth Knust, Michaela Yuan (Max-Planck-Institute of Molecular Cell Biology and Genetics, Dresden, Germany), and Xavier Bailly (Center National de la Recherche Scientifique & Université Pierre et Marie Curie, CNRS-PMC, Roscoff, France) for their help with *S. roscoffensis* samples; Enrique Arboleda (Institut de Génomique Fonctionnelle de Lyon, IGFL, Lyon, France) for helping with the embryos of *P. hawaiensis*; Pedro Martinez Serra (Departament de Genética, Microbiologia i Estadística, Universitat de Barcelona, Barcelona, Spain) for his valuable suggestions; and Martin Lowe (School of Biological Sciences, Division of Molecular & Cellular Function, University of Manchester, Manchester, UK) and Evelyn Houliston (Laboratoire de Biologie du Développement de Villefranche-sur-mer, Villefranche-sur-Mer, France) for their comments on the manuscript. Part of the graphical abstract was created with BioRender. E.A. was supported by an SZN-funded fellowship (Open University – Stazione Zoologica Anton Dohrn PhD Program). The study was funded by an SZN intramural grant to F.F. and by the Italian Ministry of University and Research PRIN-2022 grant (CUP project code C53D23003000006; MUR project code 20222SKZEE) to M.I.A.

AUTHOR CONTRIBUTIONS

Conceptualization, F.F.; methodology, F.F., M.I.A., S.D., and S.L.; investigation, F.F., G.B., S.L., E.A., and S. Bormke; resources, S.J., M.K., K.M., V.H., V.B., H.E., S. Bertrand, C.L., J.U.-L., B.S., P.B., I.R.-T., G.J., and E.D.; writing – original draft, F.F.; writing – review & editing, F.F., G.B., S.L., H.E., S. Bertrand, S.D., J.U.-L., C.L., I.R.-T., B.S., G.J., P.B., and M.I.A.; visualization, F.F.; supervision, F.F.

DECLARATION OF INTERESTS

The authors declare no competing interests.

DECLARATION OF GENERATIVE AI AND AI-ASSISTED TECHNOLOGIES IN THE WRITING PROCESS

The authors used ChatGPT (https://chat.openai.com/) to generate the highlights and eTOC sections for this publication and take full responsibility for their content.

Received: May 11, 2023
Revised: October 31, 2023
Accepted: January 29, 2024

REFERENCES

1. Glick, B.S., and Nakano, A. (2009). Membrane traffic within the Golgi apparatus. Annu. Rev. Cell Dev. Biol. *25*, 113–132.
2. Di Martino, R., Sticco, L., and Luini, A. (2019). Regulation of cargo export and sorting at the trans-Golgi network. FEBS Lett. *593*, 2306–2318. https://doi.org/10.1002/1873-3468.13572.
3. Taniguchi, M., and Yoshida, H. (2017). TFE3, HSP47, and CREB3 Pathways of the Mammalian Golgi Stress Response. Cell Struct. Funct. *42*, 27–36. https://doi.org/10.1247/csf.16023.
4. Machamer, C.E. (2015). The Golgi complex in stress and death. Front. Neurosci. *9*, 421. https://doi.org/10.3389/fnins.2015.00421.
5. Chiu, R., Novikov, L., Mukherjee, S., and Shields, D. (2002). A caspase cleavage fragment of p115 induces fragmentation of the Golgi apparatus and apoptosis. J. Cell Biol. *159*, 637–648. https://doi.org/10.1083/jcb.200208013.
6. Mukherjee, S., Chiu, R., Leung, S.M., and Shields, D. (2007). Fragmentation of the Golgi apparatus: an early apoptotic event independent of the cytoskeleton. Traffic *8*, 369–378. https://doi.org/10.1111/j.1600-0854.2007.00542.x.
7. Tao, Y., Yang, Y., Zhou, R., and Gong, T. (2020). Golgi Apparatus: An Emerging Platform for Innate Immunity. Trends Cell Biol. *30*, 467–477. https://doi.org/10.1016/j.tcb.2020.02.008.
8. Eisenberg-Lerner, A., Benyair, R., Hizkiahou, N., Nudel, N., Maor, R., Kramer, M.P., Shmueli, M.D., Zigdon, I., Cherniavsky Lev, M., Ulman, A., et al. (2020). Golgi organization is regulated by proteasomal degradation. Nat. Commun. *11*, 409. https://doi.org/10.1038/s41467-019-14038-9.
9. Farber-Katz, S.E., Dippold, H.C., Buschman, M.D., Peterman, M.C., Xing, M., Noakes, C.J., Tat, J., Ng, M.M., Rahajeng, J., Cowan, D.M., et al. (2014). DNA damage triggers Golgi dispersal via DNA-PK and GOLPH3. Cell *156*, 413–427. https://doi.org/10.1016/j.cell.2013.12.023.
10. Catara, G., Grimaldi, G., Schembri, L., Spano, D., Turacchio, G., Lo Monte, M., Beccari, A.R., Valente, C., and Corda, D. (2017). PARP1-produced poly-ADP-ribose causes the PARP12 translocation to stress granules and impairment of Golgi complex functions. Sci. Rep. *7*, 14035. https://doi.org/10.1038/s41598-017-14156-8.
11. Mazzarello, P., Garbarino, C., and Calligaro, A. (2009). How Camillo Golgi became "the Golgi. FEBS Lett. *583*, 3732–3737. https://doi.org/10.1016/j.febslet.2009.10.018.
12. Wei, J.H., and Seemann, J. (2017). Golgi ribbon disassembly during mitosis, differentiation and disease progression. Curr. Opin. Cell Biol. *47*, 43–51. https://doi.org/10.1016/j.ceb.2017.03.008.

13. Gosavi, P., and Gleeson, P.A. (2017). The Function of the Golgi Ribbon Structure - An Enduring Mystery Unfolds!. Bioessays *39*. https://doi.org/10.1002/bies.201700063.

14. Ayala, I., Mascanzoni, F., and Colanzi, A. (2020). The Golgi ribbon: mechanisms of maintenance and disassembly during the cell cycle. Biochem. Soc. Trans. *48*, 245–256. https://doi.org/10.1042/BST20190646.

15. Haase, G., and Rabouille, C. (2015). Golgi Fragmentation in ALS Motor Neurons. New Mechanisms Targeting Microtubules, Tethers, and Transport Vesicles. Front. Neurosci. *9*, 448. https://doi.org/10.3389/fnins.2015.00448.

16. Joshi, G., Chi, Y., Huang, Z., and Wang, Y. (2014). Abeta-induced Golgi fragmentation in Alzheimer's disease enhances Abeta production. Proc. Natl. Acad. Sci. USA *111*, E1230–E1239. https://doi.org/10.1073/pnas.1320192111.

17. Bui, S., Mejia, I., Díaz, B., and Wang, Y. (2021). Adaptation of the Golgi Apparatus in Cancer Cell Invasion and Metastasis. Front. Cell Dev. Biol. *9*, 806482. https://doi.org/10.3389/fcell.2021.806482.

18. Cortese, M., Lee, J.Y., Cerikan, B., Neufeldt, C.J., Oorschot, V.M.J., Köhrer, S., Hennies, J., Schieber, N.L., Ronchi, P., Mizzon, G., et al. (2020). Integrative Imaging Reveals SARS-CoV-2-Induced Reshaping of Subcellular Morphologies. Cell Host Microbe *28*, 853–866.e5. https://doi.org/10.1016/j.chom.2020.11.003.

19. Haukedal, H., Corsi, G.I., Gadekar, V.P., Doncheva, N.T., Kedia, S., de Haan, N., Chandrasekaran, A., Jensen, P., Schiønning, P., Vallin, S., et al. (2023). Golgi fragmentation - One of the earliest organelle phenotypes in Alzheimer's disease neurons. Front. Neurosci. *17*, 1120086. https://doi.org/10.3389/fnins.2023.1120086.

20. Eldon, E.D., Montpetit, I.C., Nguyen, T., Decker, G., Valdizan, M.C., Klein, W.H., and Brandhorst, B.P. (1990). Localization of the sea urchin Spec3 protein to cilia and Golgi complexes of embryonic ectoderm cells. Genes Dev. *4*, 111–122. https://doi.org/10.1101/gad.4.1.111.

21. Terasaki, M. (2000). Dynamics of the endoplasmic reticulum and golgi apparatus during early sea urchin development. Mol. Biol. Cell *11*, 897–914.

22. Cole, N.B., Smith, C.L., Sciaky, N., Terasaki, M., Edidin, M., and Lippincott-Schwartz, J. (1996). Diffusional mobility of Golgi proteins in membranes of living cells. Science (New York, N.Y *273*, 797–801. https://doi.org/10.1126/science.273.5276.797.

23. Ladinsky, M.S., Mastronarde, D.N., McIntosh, J.R., Howell, K.E., and Staehelin, L.A. (1999). Golgi structure in three dimensions: functional insights from the normal rat kidney cell. J. Cell Biol. *144*, 1135–1149.

24. Kondylis, V., van Nispen tot Pannerden, H.E., Herpers, B., Friggi-Grelin, F., and Rabouille, C. (2007). The golgi comprises a paired stack that is separated at G2 by modulation of the actin cytoskeleton through Abi and Scar/WAVE. Dev. Cell *12*, 901–915.

25. Yano, H., Yamamoto-Hino, M., Abe, M., Kuwahara, R., Haraguchi, S., Kusaka, I., Awano, W., Kinoshita-Toyoda, A., Toyoda, H., and Goto, S. (2005). Distinct functional units of the Golgi complex in Drosophila cells. Proc. Natl. Acad. Sci. USA *102*, 13467–13472. https://doi.org/10.1073/pnas.0506681102.

26. Page, K.M., McCormack, J.J., Lopes-da-Silva, M., Patella, F., Harrison-Lavoie, K., Burden, J.J., Quah, Y.Y.B., Scaglioni, D., Ferraro, F., and Cutler, D.F. (2022). Structure modeling hints at a granular organization of the Golgi ribbon. BMC Biol. *20*, 111. https://doi.org/10.1186/s12915-022-01305-3.

27. Lu, Z., Joseph, D., Bugnard, E., Zaal, K.J., and Ralston, E. (2001). Golgi complex reorganization during muscle differentiation: visualization in living cells and mechanism. Mol. Biol. Cell *12*, 795–808.

28. Gunn, P.A., Gliddon, B.L., Londrigan, S.L., Lew, A.M., van Driel, I.R., and Gleeson, P.A. (2011). The Golgi apparatus in the endomembrane-rich gastric parietal cells exist as functional stable mini-stacks dispersed throughout the cytoplasm. Biol. Cell. *103*, 559–572. https://doi.org/10.1042/BC20110074.

29. Koga, D., and Ushiki, T. (2006). Three-dimensional ultrastructure of the Golgi apparatus in different cells: high-resolution scanning electron microscopy of osmium-macerated tissues. Arch. Histol. Cytol. *69*, 357–374. https://doi.org/10.1679/aohc.69.357.

30. Wandall, H.H., Rumjantseva, V., Sørensen, A.L.T., Patel-Hett, S., Josefsson, E.C., Bennett, E.P., Italiano, J.E., Jr., Clausen, H., Hartwig, J.H., and Hoffmeister, K.M. (2012). The origin and function of platelet glycosyltransferases. Blood *120*, 626–635. https://doi.org/10.1182/blood-2012-02-409235.

31. Ramón y Cajal, S. (1903). Sobre la existencia de un aparato tubuliforme en el protoplasma de las células nerviosas y epiteliales de la lombriz de tierra (Boletín de la Sociedad Española de Historia Natural), pp. 395–398.

32. Perroncito, A. (1910). Contributo allo studio della biologia cellulare – mitocondri, cromidii e apparato reticolare interno nelle cellule spermatiche. Memorie della R. Accademia dei Lincei; Classe di Scienze Fisiche, Matematiche e Naturali *VIII*, 226–261.

33. Mollenhauer, H.H., and Morré, D.J. (1998). The tubular network of the Golgi apparatus. Histochem. Cell Biol. *109*, 533–543. https://doi.org/10.1007/s004180050253.

34. Meek, G.A., and Bradbury, S. (1963). Localization of thiamine pyrophosphatase activity in the golgi apparatus of a mollusc, Helix aspersa. J. Cell Biol. *18*, 73–85. https://doi.org/10.1083/jcb.18.1.73.

35. Sato, M., Saegusa, K., Sato, K., Hara, T., Harada, A., and Sato, K. (2011). Caenorhabditis elegans SNAP-29 is required for organellar integrity of the endomembrane system and general exocytosis in intestinal epithelial cells. Mol. Biol. Cell *22*, 2579–2587. https://doi.org/10.1091/mbc.E11-04-0279.

36. Kuterbach, D.A., and Walcott, B. (1986). Iron-containing cells in the honey-bee (Apis mellifera). I. Adult morphology and physiology. J. Exp. Biol. *126*, 375–387. https://doi.org/10.1242/jeb.126.1.375.

37. Griffiths, G.W., and Beck, S.D. (1975). Ultrastructure of pea aphid mycetocytes: evidence for symbiote secretion. Cell Tissue Res. *159*, 351–367. https://doi.org/10.1007/BF00221782.

38. Rolls, M.M., Marquardt, M.T., Kielian, M., and Machamer, C.E. (1997). Cholesterol-independent targeting of Golgi membrane proteins in insect cells. Mol. Biol. Cell *8*, 2111–2118. https://doi.org/10.1091/mbc.8.11.2111.

39. Van-Praët, M. (1985). Nutrition of Sea Anemones. Adv. Mar. Biol. *22*, 65–99. https://doi.org/10.1016/S0065-2881(08)60050-4.

40. Romanova, D.Y., Varoqueaux, F., Daraspe, J., Nikitin, M.A., Eitel, M., Fasshauer, D., and Moroz, L.L. (2021). Hidden cell diversity in Placozoa: ultrastructural insights from Hoilungia hongkongensis. Cell Tissue Res. *385*, 623–637. https://doi.org/10.1007/s00441-021-03459-y.

41. Laundon, D., Larson, B.T., McDonald, K., King, N., and Burkhardt, P. (2019). The architecture of cell differentiation in choanoflagellates and sponge choanocytes. PLoS Biol. *17*, e3000226. https://doi.org/10.1371/journal.pbio.3000226.

42. Burkhardt, P., Stegmann, C.M., Cooper, B., Kloepper, T.H., Imig, C., Varoqueaux, F., Wahl, M.C., and Fasshauer, D. (2011). Primordial neurosecretory apparatus identified in the choanoflagellate Monosiga brevicollis. Proc. Natl. Acad. Sci. USA *108*, 15264–15269. https://doi.org/10.1073/pnas.1106189108.

43. Harrison, F.W., and De Vos, L. (1991). Porifera. Microscopic Anatomy of Invertebrates: Placozoa, Porifera, Cnidaria, and Ctenophora, *2* (Willey-Liss (Willey-Liss).

44. Witkos, T.M., and Lowe, M. (2015). The Golgin Family of Coiled-Coil Tethering Proteins. Front. Cell Dev. Biol. *3*, 86. https://doi.org/10.3389/fcell.2015.00086.

45. Kulkarni-Gosavi, P., Makhoul, C., and Gleeson, P.A. (2019). Form and function of the Golgi apparatus: scaffolds, cytoskeleton and signalling. FEBS Lett. *593*, 2289–2305. https://doi.org/10.1002/1873-3468.13567.

46. Bekier, M.E., 2nd, Wang, L., Li, J., Huang, H., Tang, D., Zhang, X., and Wang, Y. (2017). Knockout of the Golgi stacking proteins GRASP55

and GRASP65 impairs Golgi structure and function. Mol. Biol. Cell *28*, 2833–2842. https://doi.org/10.1091/mbc.E17-02-0112.

47. Grond, R., Veenendaal, T., Duran, J.M., Raote, I., van Es, J.H., Corstjens, S., Delfgou, L., El Haddouti, B., Malhotra, V., and Rabouille, C. (2020). The function of GORASPs in Golgi apparatus organization in vivo. J. Cell Biol. *219*, e202004191. https://doi.org/10.1083/jcb.202004191.
48. Zhang, Y., and Seemann, J. (2021). Rapid degradation of GRASP55 and GRASP65 reveals their immediate impact on the Golgi structure. J. Cell Biol. *220*, e202007052. https://doi.org/10.1083/jcb.202007052.
49. Kinseth, M.A., Anjard, C., Fuller, D., Guizzunti, G., Loomis, W.F., and Malhotra, V. (2007). The Golgi-associated protein GRASP is required for unconventional protein secretion during development. Cell *130*, 524–534. https://doi.org/10.1016/j.cell.2007.06.029.
50. Zhang, X., Wang, L., Lak, B., Li, J., Jokitalo, E., and Wang, Y. (2018). GRASP55 Senses Glucose Deprivation through O-GlcNAcylation to Promote Autophagosome-Lysosome Fusion. Dev. Cell *45*, 245–261.e6. https://doi.org/10.1016/j.devcel.2018.03.023.
51. Nüchel, J., Tauber, M., Nolte, J.L., Mörgelin, M., Türk, C., Eckes, B., Demetriades, C., and Plomann, M. (2021). An mTORC1-GRASP55 signaling axis controls unconventional secretion to reshape the extracellular proteome upon stress. Mol. Cell *81*, 3275–3293.e12. https://doi.org/10.1016/j.molcel.2021.06.017.
52. Rabouille, C., and Linstedt, A.D. (2016). GRASP: A Multitasking Tether. Front. Cell Dev. Biol. *4*, 1. https://doi.org/10.3389/fcell.2016.00001.
53. Pothukuchi, P., Agliarulo, I., Pirozzi, M., Rizzo, R., Russo, D., Turacchio, G., Nüchel, J., Yang, J.S., Gehin, C., Capolupo, L., et al. (2021). GRASP55 regulates intra-Golgi localization of glycosylation enzymes to control glycosphingolipid biosynthesis. EMBO J. *40*, e107766. https://doi.org/10.15252/embj.2021107766.
54. Luo, Q., Liu, Q., Cheng, H., Wang, J., Zhao, T., Zhang, J., Mu, C., Meng, Y., Chen, L., Zhou, C., et al. (2022). Nondegradable ubiquitinated ATG9A organizes Golgi integrity and dynamics upon stresses. Cell Rep. *40*, 111195. https://doi.org/10.1016/j.celrep.2022.111195.
55. Xiang, Y., and Wang, Y. (2010). GRASP55 and GRASP65 play complementary and essential roles in Golgi cisternal stacking. J. Cell Biol. *188*, 237–251. https://doi.org/10.1083/jcb.200907132.
56. Barr, F.A., Puype, M., Vandekerckhove, J., and Warren, G. (1997). GRASP65, a protein involved in the stacking of Golgi cisternae. Cell *91*, 253–262.
57. Shorter, J., Watson, R., Giannakou, M.E., Clarke, M., Warren, G., and Barr, F.A. (1999). GRASP55, a second mammalian GRASP protein involved in the stacking of Golgi cisternae in a cell-free system. EMBO J. *18*, 4949–4960. https://doi.org/10.1093/emboj/18.18.4949.
58. Kuo, A., Zhong, C., Lane, W.S., and Derynck, R. (2000). Transmembrane transforming growth factor-alpha tethers to the PDZ domain-containing, Golgi membrane-associated protein p59/GRASP55. EMBO J. *19*, 6427–6439. https://doi.org/10.1093/emboj/19.23.6427.
59. Barr, F.A., Nakamura, N., and Warren, G. (1998). Mapping the interaction between GRASP65 and GM130, components of a protein complex involved in the stacking of Golgi cisternae. EMBO J. *17*, 3258–3268. https://doi.org/10.1093/emboj/17.12.3258.
60. Short, B., Preisinger, C., Körner, R., Kopajtich, R., Byron, O., and Barr, F.A. (2001). A GRASP55-rab2 effector complex linking Golgi structure to membrane traffic. J. Cell Biol. *155*, 877–883. https://doi.org/10.1083/jcb.200108079.
61. Sengupta, D., Truschel, S., Bachert, C., and Linstedt, A.D. (2009). Organelle tethering by a homotypic PDZ interaction underlies formation of the Golgi membrane network. J. Cell Biol. *186*, 41–55. https://doi.org/10.1083/jcb.200902110.
62. Bachert, C., and Linstedt, A.D. (2010). Dual anchoring of the GRASP membrane tether promotes trans pairing. J. Biol. Chem. *285*, 16294–16301. https://doi.org/10.1074/jbc.M110.116129.
63. Heinrich, F., Nanda, H., Goh, H.Z., Bachert, C., Lösche, M., and Linstedt, A.D. (2014). Myristoylation restricts orientation of the GRASP domain on membranes and promotes membrane tethering. J. Biol. Chem. *289*, 9683–9691. https://doi.org/10.1074/jbc.M113.543561.
64. Malsam, J., Satoh, A., Pelletier, L., and Warren, G. (2005). Golgin tethers define subpopulations of COPI vesicles. Science (New York, N.Y *307*, 1095–1098. https://doi.org/10.1126/science.1108061.
65. Wong, M., and Munro, S. (2014). Membrane trafficking. The specificity of vesicle traffic to the Golgi is encoded in the golgin coiled-coil proteins. Science (New York, N.Y *346*, 1256898. https://doi.org/10.1126/science.1256898.
66. Puthenveedu, M.A., Bachert, C., Puri, S., Lanni, F., and Linstedt, A.D. (2006). GM130 and GRASP65-dependent lateral cisternal fusion allows uniform Golgi-enzyme distribution. Nat. Cell Biol. *8*, 238–248. https://doi.org/10.1038/ncb1366.
67. Zhao, J., Li, B., Huang, X., Morelli, X., and Shi, N. (2017). Structural Basis for the Interaction between Golgi Reassembly-stacking Protein GRASP55 and Golgin45. J. Biol. Chem. *292*, 2956–2965. https://doi.org/10.1074/jbc.M116.765990.
68. Hu, F., Shi, X., Li, B., Huang, X., Morelli, X., and Shi, N. (2015). Structural basis for the interaction between the Golgi reassembly-stacking protein GRASP65 and the Golgi matrix protein GM130. J. Biol. Chem. *290*, 26373–26382. https://doi.org/10.1074/jbc.M115.657940.
69. Barlow, L.D., Nývltová, E., Aguilar, M., Tachezy, J., and Dacks, J.B. (2018). A sophisticated, differentiated Golgi in the ancestor of eukaryotes. BMC Biol. *16*, 27. https://doi.org/10.1186/s12915-018-0492-9.
70. Jumper, J., Evans, R., Pritzel, A., Green, T., Figurnov, M., Ronneberger, O., Tunyasuvunakool, K., Bates, R., Žídek, A., Potapenko, A., et al. (2021). Highly accurate protein structure prediction with AlphaFold. Nature *596*, 583–589. https://doi.org/10.1038/s41586-021-03819-2.
71. Mirdita, M., Schütze, K., Moriwaki, Y., Heo, L., Ovchinnikov, S., and Steinegger, M. (2022). ColabFold: making protein folding accessible to all. Nat. Methods *19*, 679–682. https://doi.org/10.1038/s41592-022-01488-1.
72. Tsaban, T., Varga, J.K., Avraham, O., Ben-Aharon, Z., Khramushin, A., and Schueler-Furman, O. (2022). Harnessing protein folding neural networks for peptide-protein docking. Nat. Commun. *13*, 176. https://doi.org/10.1038/s41467-021-27838-9.
73. Guo, H.B., Perminov, A., Bekele, S., Kedziora, G., Farajollahi, S., Varaljay, V., Hinkle, K., Molinero, V., Meister, K., Hung, C., et al. (2022). AlphaFold2 models indicate that protein sequence determines both structure and dynamics. Sci. Rep. *12*, 10696. https://doi.org/10.1038/s41598-022-14382-9.
74. Johansson-Åkhe, I., and Wallner, B. (2022). Improving peptide-protein docking with AlphaFold-Multimer using forced sampling. Front. Bioinform. *2*, 959160. https://doi.org/10.3389/fbinf.2022.959160.
75. Thyberg, J., and Moskalewski, S. (1985). Microtubules and the organization of the Golgi complex. Exp. Cell Res. *159*, 1–16.
76. Cole, N.B., Sciaky, N., Marotta, A., Song, J., and Lippincott-Schwartz, J. (1996). Golgi dispersal during microtubule disruption: regeneration of Golgi stacks at peripheral endoplasmic reticulum exit sites. Mol. Biol. Cell *7*, 631–650.
77. Kiyonari, H., Kaneko, M., Abe, T., Shioi, G., Aizawa, S., Furuta, Y., and Fujimori, T. (2019). Dynamic organelle localization and cytoskeletal reorganization during preimplantation mouse embryo development revealed by live imaging of genetically encoded fluorescent fusion proteins. Genesis *57*, e23277. https://doi.org/10.1002/dvg.23277.
78. Davidson, E.H., Cameron, R.A., and Ransick, A. (1998). Specification of cell fate in the sea urchin embryo: summary and some proposed mechanisms. Development *125*, 3269–3290. https://doi.org/10.1242/dev.125.17.3269.
79. Makhoul, C., Gosavi, P., and Gleeson, P.A. (2019). Golgi Dynamics: The Morphology of the Mammalian Golgi Apparatus in Health and Disease. Front. Cell Dev. Biol. *7*, 112. https://doi.org/10.3389/fcell.2019.00112.

80. Mendes, L.F.S., Batista, M.R.B., Kava, E., Bleicher, L., Micheletto, M.C., and Costa-Filho, A.J. (2022). Resurrecting Golgi proteins to grasp Golgi ribbon formation and self-association under stress. Int. J. Biol. Macromol. *194*, 264–275. https://doi.org/10.1016/j.ijbiomac.2021.11.173.

81. Knoll, A.H. (2011). The Multiple Origins of Complex Multicellularity. Annu. Rev. Earth Planet Sci. *39*, 217–239. https://doi.org/10.1146/annurev.earth.031208.100209.

82. Staehelin, L.A., and Kang, B.H. (2008). Nanoscale architecture of endoplasmic reticulum export sites and of Golgi membranes as determined by electron tomography. Plant Physiol. *147*, 1454–1468. https://doi.org/10.1104/pp.108.120618.

83. Bracker, C.E., James Morré, D., and Grove, S.N. (1996). Structure, differentiation, and multiplication of Golgi apparatus in fungal hyphae. Protoplasma *194*, 250–274.

84. Dumitru, R., Gama, V., Fagan, B.M., Bower, J.J., Swahari, V., Pevny, L.H., and Deshmukh, M. (2012). Human embryonic stem cells have constitutively active Bax at the Golgi and are primed to undergo rapid apoptosis. Mol. Cell *46*, 573–583. https://doi.org/10.1016/j.molcel.2012.04.002.

85. Christoforou, A., Mulvey, C.M., Breckels, L.M., Geladaki, A., Hurrell, T., Hayward, P.C., Naake, T., Gatto, L., Viner, R., Martinez Arias, A., and Lilley, K.S. (2016). A draft map of the mouse pluripotent stem cell spatial proteome. Nat. Commun. *7*, 8992. https://doi.org/10.1038/ncomms9992.

86. Lemonnier, T., Blanchard, S., Toli, D., Roy, E., Bigou, S., Froissart, R., Rouvet, I., Vitry, S., Heard, J.M., and Bohl, D. (2011). Modeling neuronal defects associated with a lysosomal disorder using patient-derived induced pluripotent stem cells. Hum. Mol. Genet. *20*, 3653–3666. https://doi.org/10.1093/hmg/ddr285.

87. Huangfu, D., Osafune, K., Maehr, R., Guo, W., Eijkelenboom, A., Chen, S., Muhlestein, W., and Melton, D.A. (2008). Induction of pluripotent stem cells from primary human fibroblasts with only Oct4 and Sox2. Nat. Biotechnol. *26*, 1269–1275. https://doi.org/10.1038/nbt.1502.

88. Gendarme, M., Baumann, J., Ignashkova, T.I., Lindemann, R.K., and Reiling, J.H. (2017). Image-based drug screen identifies HDAC inhibitors as novel Golgi disruptors synergizing with JQ1. Mol. Biol. Cell *28*, 3756–3772. https://doi.org/10.1091/mbc.E17-03-0176.

89. Houliston, E., Leclère, L., Munro, C., Copley, R.R., and Momose, T. (2022). Past, present and future of Clytia hemisphaerica as a laboratory jellyfish. Curr. Top. Dev. Biol. *147*, 121–151. https://doi.org/10.1016/bs.ctdb.2021.12.014.

90. Darling, J.A., Reitzel, A.R., Burton, P.M., Mazza, M.E., Ryan, J.F., Sullivan, J.C., and Finnerty, J.R. (2005). Rising starlet: the starlet sea anemone, Nematostella vectensis. Bioessays *27*, 211–221. https://doi.org/10.1002/bies.20181.

91. Özpolat, B.D., Randel, N., Williams, E.A., Bezares-Calderón, L.A., Andreatta, G., Balavoine, G., Bertucci, P.Y., Ferrier, D.E.K., Gambi, M.C., Gazave, E., et al. (2021). The Nereid on the rise: Platynereis as a model system. EvoDevo *12*, 10. https://doi.org/10.1186/s13227-021-00180-3.

92. Mendes, L.F.S., Fontana, N.A., Reddy, S.T., Uversky, V.N., and Costa-Filho, A.J. (2020). The exquisite structural biophysics of the Golgi Reassembly and Stacking Proteins. Int. J. Biol. Macromol. *164*, 3632–3644. https://doi.org/10.1016/j.ijbiomac.2020.08.203.

93. Hertel, L.A., Bayne, C.J., and Loker, E.S. (2002). The symbiont Capsaspora owczarzaki, nov. gen. nov. sp., isolated from three strains of the pulmonate snail Biomphalaria glabrata is related to members of the Mesomycetozoea. Int. J. Parasitol. *32*, 1183–1191. https://doi.org/10.1016/s0020-7519(02)00066-8.

94. Minh, B.Q., Schmidt, H.A., Chernomor, O., Schrempf, D., Woodhams, M.D., von Haeseler, A., and Lanfear, R. (2020). IQ-TREE 2: New Models and Efficient Methods for Phylogenetic Inference in the Genomic Era. Mol. Biol. Evol. *37*, 1530–1534. https://doi.org/10.1093/molbev/msaa015.

95. Kalyaanamoorthy, S., Minh, B.Q., Wong, T.K.F., von Haeseler, A., and Jermiin, L.S. (2017). ModelFinder: fast model selection for accurate phylogenetic estimates. Nat. Methods *14*, 587–589. https://doi.org/10.1038/nmeth.4285.

96. Paganos, P., Caccavale, F., La Vecchia, C., D'Aniello, E., D'Aniello, S., and Arnone, M.I. (2022). FISH for All: A Fast and Efficient Fluorescent In situ Hybridization (FISH) Protocol for Marine Embryos and Larvae. Front. Physiol. *13*, 878062. https://doi.org/10.3389/fphys.2022.878062.

97. Reed, C.G. (1987). Reproduction and development of marine invertebrates of the northern Pacific coast. Phylum Brachiopoda (University of Washington Press).

98. Nislow, C. (1994). Reproduction and Development of Marine Invertebrates. Cellular Dynamics during the Early Development of an Articulate Brachiopod (Johns Hopkins University Press).

99. Sachkova, M.Y., Nordmann, E.L., Soto-Àngel, J.J., Meeda, Y., Górski, B., Naumann, B., Dondorp, D., Chatzigeorgiou, M., Kittelmann, M., and Burkhardt, P. (2021). Neuropeptide repertoire and 3D anatomy of the ctenophore nervous system. Curr. Biol. *31*, 5274–5285.e6. https://doi.org/10.1016/j.cub.2021.09.005.

100. Schierwater, B. (2005). My favorite animal, Trichoplax adhaerens. Bioessays *27*, 1294–1302. https://doi.org/10.1002/bies.20320.

101. Ferraro, F., Patella, F., Costa, J.R., Ketteler, R., Kriston-Vizi, J., and Cutler, D.F. (2020). Modulation of endothelial organelle size as an antithrombotic strategy. J. Thromb. Haemostasis *18*, 3296–3308. https://doi.org/10.1111/jth.15084.

102. Paganos, P., Ronchi, P., Carl, J., Mizzon, G., Martinez, P., Benvenuto, G., and Arnone, M.I. (2022). Integrating single cell transcriptomics and volume electron microscopy confirms the presence of pancreatic acinar-like cells in sea urchins. Front. Cell Dev. Biol. *10*, 991664. https://doi.org/10.3389/fcell.2022.991664.

103. Sebé-Pedrós, A., Irimia, M., Del Campo, J., Parra-Acero, H., Russ, C., Nusbaum, C., Blencowe, B.J., and Ruiz-Trillo, I. (2013). Regulated aggregative multicellularity in a close unicellular relative of metazoa. Elife *2*, e01287. https://doi.org/10.7554/eLife.01287.

104. Verasztó, C., Jasek, S., Gühmann, M., Shahidi, R., Ueda, N., Beard, J.D., Mendes, S., Heinz, K., Bezares-Calderón, L.A., Williams, E., and Jékely, G. (2020). Whole-animal connectome and cell-type complement of the three-segmented Platynereis dumerilii larva. Preprint at bioRxiv. https://doi.org/10.1101/2020.08.21.260984.

105. Baena, V., Schalek, R.L., Lichtman, J.W., and Terasaki, M. (2019). Serial-section electron microscopy using automated tape-collecting ultramicrotome (ATUM). Methods Cell Biol. *152*, 41–67. https://doi.org/10.1016/bs.mcb.2019.04.004.

106. Richter, D.J., Fozouni, P., Eisen, M.B., and King, N. (2018). Gene family innovation, conservation and loss on the animal stem lineage. Elife *7*, e34226. https://doi.org/10.7554/eLife.34226.

107. Steinegger, M., and Söding, J. (2017). MMseqs2 enables sensitive protein sequence searching for the analysis of massive data sets. Nat. Biotechnol. *35*, 1026–1028. https://doi.org/10.1038/nbt.3988.

108. Akdel, M., Pires, D.E.V., Pardo, E.P., Jänes, J., Zalevsky, A.O., Mészáros, B., Bryant, P., Good, L.L., Laskowski, R.A., Pozzati, G., et al. (2022). A structural biology community assessment of AlphaFold2 applications. Nat. Struct. Mol. Biol. *29*, 1056–1067. https://doi.org/10.1038/s41594-022-00849-w.

109. Tunyasuvunakool, K., Adler, J., Wu, Z., Green, T., Zielinski, M., Žídek, A., Bridgland, A., Cowie, A., Meyer, C., Laydon, A., et al. (2021). Highly accurate protein structure prediction for the human proteome. Nature *596*, 590–596. https://doi.org/10.1038/s41586-021-03828-1.

110. Ruff, K.M., and Pappu, R.V. (2021). AlphaFold and Implications for Intrinsically Disordered Proteins. J. Mol. Biol. *433*, 167208. https://doi.org/10.1016/j.jmb.2021.167208.

111. Tie, H.C., Ludwig, A., Sandin, S., and Lu, L. (2018). The spatial separation of processing and transport functions to the interior and periphery of the Golgi stack. Elife *7*, e41301. https://doi.org/10.7554/eLife.41301.

112. Feuda, R., Dohrmann, M., Pett, W., Philippe, H., Rota-Stabelli, O., Lartillot, N., Wörheide, G., and Pisani, D. (2017). Improved Modeling of Compositional Heterogeneity Supports Sponges as Sister to All Other Animals. Curr. Biol. *27*, 3864–3870.e4. https://doi.org/10.1016/j.cub.2017.11.008.

113. Borowiec, M.L., Lee, E.K., Chiu, J.C., and Plachetzki, D.C. (2015). Extracting phylogenetic signal and accounting for bias in whole-genome data sets supports the Ctenophora as sister to remaining Metazoa. BMC Genom. *16*, 987. https://doi.org/10.1186/s12864-015-2146-4.

114. Dellaporta, S.L., Xu, A., Sagasser, S., Jakob, W., Moreno, M.A., Buss, L.W., and Schierwater, B. (2006). Mitochondrial genome of Trichoplax adhaerens supports placozoa as the basal lower metazoan phylum. Proc. Natl. Acad. Sci. USA *103*, 8751–8756. https://doi.org/10.1073/pnas.0602076103.

Please cite this article in press as: Benvenuto et al., Evolution of the ribbon-like organization of the Golgi apparatus in animal cells, Cell Reports (2024), https://doi.org/10.1016/j.celrep.2024.113791

STAR★METHODS

KEY RESOURCES TABLE

REAGENT or RESOURCE	SOURCE	IDENTIFIER
Antibodies		
Mouse monoclonal anti-GM130 (clone 35)	BD Biosciences	Cat# 610823; RRID: AB_398142
Bacterial strains		
One Shot™ TOP10 Chemically Competent *E. coli*	ThermoFisher	Cat# C404010
Chemicals		
DMSO, Hybri-Max™	Merck Millipore/Sigma-Aldrich	Cat# D2650
Nocodazole	Merck Millipore/Sigma-Aldrich	Cat# M1404
Commercial assays		
mMESSAGE mMACHINE T7 transcription kit	Invitrogen	Cat# AM1344
NEBuilder HiFi DNA assembly cloning kit	NEB	Cat# E5520
Q5® High-Fidelity DNA polymerase	NEB	Cat# M0491
Experimental models: Cell lines		
Human Umbilical Vein Endothelial Cells (HUVECs) pooled donors	Promocell	Cat. No. C-12203
Experimental models: Organisms/strains		
Paracentrotus lividus – wild type	Gulf of Naples, Italy	N/A
Strongylocentrotus purpuratus – wild type	California, USA	N/A
Ciona robusta – wild type	Gulf of Taranto, Italy	N/A
Branchiostoma lanceolatum – wild type	Argelès-sur-mer, France	N/A
Platynereis dumerilii – wild type	Cultured colony (founders from the Gulf of Naples)	N/A
Calloria inconspicua – wild type	Karitane Point, New Zealand	N/A
Clytia hemisphaerica – wild type Z strain	Cultured colony Leclère et al. 2019 https://doi.org/10.1038/s41559-019-0833-2	N/A
Symsagittifera roscoffensis – wild type	Roscoff, Brittany, France	N/A
Parhyale hawaiensis – wild type	Cultured colony (founders from the John G. Shedd Aquarium; Chicago; USA)	N/A
Trichoplax adhaerens – wild type	Cultured clone (originally sourced from the Red Sea)	N/A
Mnemiopsis leidyi – wild type	Kristineberg, Sweden	N/A
Oscarella carmela – wild type	Carmel, California, USA	N/A
Capsaspora owczarzaki – wild type strain	Hertel, L.A., [93].https://doi.org/10.1016/S0020-7519(02)00066-8	ATCC30864
Oligonucleotides		
Primer F 1: atacgactcactataggctagcATGGTGA GCAAGGGCGAG	This paper	N/A
Primer R 1: acctgatccaccgccCTTGTACAGC TCGTCCATGC	This paper	N/A
Primer F 2: *ctgtacaag*ggcggtggatcaggtggag gatctACTCCTATCATTGGCTC	This paper	N/A
Primer R 2: gaggtaccacgcgtgaatTCATTACT ATAGATGGCCC	This paper	N/A
Primer F 3: ttaatacgactcactataggctagcATGAGG CTTCGGGAGCCG	This paper	N/A

(*Continued on next page*)

Continued

REAGENT or RESOURCE	SOURCE	IDENTIFIER
Primer R 3: ctctagaggtaccacgcgtgaattcTTACTTG TACAGCTCGTCCATGC	This paper	N/A
Primer F 4: ttaatacgactcactataggctagcATGGTG AGCAAGGGCGAG	This paper	N/A
Primer R 4: ctctagaggtaccacgcgtg*aattcttacataatt acacactttgtctttgacttctttttcttctttttacc*CTTGTA CAGCTCGTCCATGC	This paper	N/A
Recombinant DNA		
Plasmid: pCineo vector	Promega	Cat# E1841
Plasmid: pCineo_mEGFP_Giant-CT	This paper	N/A
Plasmid: pCineo_mCherry_CAAX	This paper	N/A
Plasmid: pCineo_GalT_mCherry	This paper	N/A
Software and algorithms		
ImageJ	Schindelin, J. et al. 2012 https://doi.org/10.1038/nmeth.2019	https://imagej.net/ij/index.html
Prism v9.4.1	N/A	https://www.graphpad.com/
BLAST	N/A	https://blast.ncbi.nlm.nih.gov/Blast.cgi
CLUSTAL-omega	Sievers, F. et al., 2011 https://doi.org/10.1038/msb.2011.75	https://www.ebi.ac.uk/Tools/msa/clustalo/
AliView	Larsson, A., 2014 https://doi.org/10.1093/bioinformatics/btu531	https://ormbunkar.se/aliview/
JalView	Waterhouse, A.M. et al., 2009 https://doi.org/10.1093/bioinformatics/btp033	https://www.jalview.org/
AlphaFold2	Jumper, J. et al., [70] https://doi.org/10.1038/s41586-021-03819-2.	https://www.deepmind.com/open-source/alphafold
ColabFold	Mirdita, M. et al., [71] https://doi.org/10.1038/s41592-022-01488-1	https://colab.research.google.com/github/sokrypton/ColabFold/blob/main/AlphaFold2.ipynb
Chimera	Pettersen E.F. et al., 2004 https://doi.org/10.1002/jcc.20084	http://www.cgl.ucsf.edu/chimera/
IQ-TREE 2	Minh B.Q. et al., [94] https://doi.org/10.1093/molbev/msaa015	http://www.iqtree.org/
ModelFinder	Kalyaanamoorthy, S. et al., [95] https://doi.org/10.1038/nmeth.4285	http://www.iqtree.org/ModelFinder/
FigTree	N/A	http://tree.bio.ed.ac.uk/software/figtree/
NEBuilder	N/A	https://nebuilder.neb.com/

RESOURCE AVAILABILITY

Lead contact

Further information and request for resources should be directed to and will be fulfilled by the lead contact, Francesco Ferraro (francesco.ferraro@szn.it).

Materials availability

All reagents generated in this study are available from the lead contact upon request.

Data and code availability

- All data reported in this study will be shared by the lead contact upon request.
- This study does not report original code.

Please cite this article in press as: Benvenuto et al., Evolution of the ribbon-like organization of the Golgi apparatus in animal cells, Cell Reports (2024), https://doi.org/10.1016/j.celrep.2024.113791

EXPERIMENTAL MODEL AND STUDY PARTICIPANT DETAILS

Paracentrotus lividus

Adult animals collected from the Gulf of Naples (Italy) were maintained in seawater circulating aquaria at Stazione Zoologica Anton Dohrn (Naples, Italy). The embryos analyzed were obtained by *in vitro* fertilization as previously described.[96]

Branchiostoma lanceolatum

This study used embryos generated by *in vitro* fertilization[96] using gametes of adults collected in Argelès-sur-mer (France) and spawned at Observatoire Océanologique de Banyuls-sur-Mer (France).

Ciona robusta

Adult animals were collected from the Gulf of Taranto (Italy) and maintained at Stazione Zoologica Anton Dohrn (Naples, Italy) as described for *Paracentrotus lividus*. The embryos and larvae analyzed were obtained by *in vitro* fertilization.[96]

Calloria inconspicua

Adults of *Calloria inconspicua* were collected at Karitane Point, South Island, New Zealand and maintained at Portobello Marine Laboratory (University of Otago) at 9°C–12°C in aquarium tanks. Artificial insemination of extracted eggs and sperm was carried out following described methods.[97,98] Developing embryos were maintained in 1 L beakers, with seawater change 1–2 times per day, until metamorphosis. Three-lobed larvae were analyzed in this study.

Strongylocentrotus purpuratus

Adult animals, collected in the Gulf of Santa Catalina (CA, United States) and distributed by Patrick Leahy (Kerckhoff Marine Laboratory, California Institute of Technology, Pasadena, CA, USA), were maintained at Stazione Zoologica Anton Dohrn (Naples, Italy). Plutei (three-day old larvae) were used in this study.

Platynereis dumerilii

Three-day old wild-type larvae from laboratory cultures were used in this study. The *Platynereis dumerilii* culture was originally established in 1950s with animals from Ischia, Italy; over the years, animals from other locations have occasionally been added to the culture.

Parhyale hawaiensis

The newly hatched embryos analyzed in this study were a gift by Michalis Averof (Institut de Génomique Fonctionnelle de Lyon, IGFL, Lyon, France). Animals, cultured in the lab, derive from specimens originally collected in 1997 by William Browne in the seawater filtration system of the Shedd Aquarium (Chicago, IL, USA).

Symsagittifera roscoffensis

Wild type adult animals were collected in Brittany near the Station Biologique de Roscoff, CNRS/Sorbonne Université, Roscoff (France). Eggs of mated adults were cultivated at 15°C in sea water. Juveniles were fixed within 3 days of hatching.

Clytia hemisphaerica

Animals were from a wild-type colony maintained in the lab and originally established with specimens collected from the bay of Villefranche-sur-Mer (France). The samples analyzed were from adult animals.

Mnemiopsis leidyi

The cydippid larvae used in this study were established and maintained at the Sars International Center for Marine Molecular Biology, University of Bergen, Bergen (Norway) as previously described.[99]

Trichoplax adhaerens

The ''Grell clone'', established by animals originally collected in the Red Sea in 1969,[100] was used in this study. Animals were maintained in glass Petri dishes in seawater at 22°C and fed with *Pyrenomonas helgolandii* algae obtained from the Culture Collection of Algae at Göttingen University (Germany).

Oscarella carmela

Specimens used in this study were collected in the sea of Carmel, CA (USA) and maintained as previously described.[41]

Capsaspora owczarzaki

The *Capsaspora* owczarzaki ATCC30864 strain, established in 2002,[93] was used. Cells were maintained in modified PYNFH medium (ATCC medium 1034) (https://www.atcc.org/products/327-x).

Please cite this article in press as: Benvenuto et al., Evolution of the ribbon-like organization of the Golgi apparatus in animal cells, Cell Reports (2024), https://doi.org/10.1016/j.celrep.2024.113791

Human umbilical vein endothelial cells

Cells collected from human umbilical cords of newborns and pooled from donors of both sexes were acquired from PromoCell. Cells expanded and maintained as previously described[101] were used within the 4th passage.

METHOD DETAILS

Plasmids

Assembly primers F1-F4 and R1-R4 (sequences in the key resources table) were designed using the NEBuilder tool (http://nebuilder.neb.com/). PCR reactions for amplicon generation were carried out with Q5 High-Fidelity DNA Polymerase (New England Biolabs). The amplicons described below and the pCineo plasmid (linearized by NheI/EcoRI digestion) were assembled using the NEBuilder HiFi DNA assembly cloning kit (New England Biolabs) following the manufacturer instructions. Correct sequences were verified by Sanger sequencing.

Plasmid pCineo_mEGFP_Giant-CT (encoding the Golgi marker mEGFP_Golgi). The plasmid encodes mEGFP in frame with a linker sequence (GGGSGGGS) and the 69 C-terminal amino acids of human Giantin for Golgi membrane targeting. The mEGFP coding sequence was amplified from pmEGFP-N1 vector (Clontech) with primers F 1 (lower case: pCineo sequence; upper case mEGFP coding sequence) and R 1 (lower case: GGGS coding sequence; upper case: mEGFP coding sequence). The sequence encoding the 69 C-terminal amino acids of human Giantin was amplified from human umbilical vein endothelial cell (HUVEC) cDNA with primers F 2 (italics: mEGFP coding sequence; lower case: GGGSGGGS linker coding sequence; upper case: Giantin coding sequence) and R 2 (lower case: pCineo sequence; upper case: Giantin coding sequence and two stop codons).

Plasmid pCineo_GalT_mCherry. A plasmid (the generous gift of Irina Kaverina, Vanderbilt School of Medicine) encoding the N-terminal 87 amino acids of galactosyltransferase (GalT), which confer Golgi localization, in frame with mCherry was used as template to amplify the GalT_mCherry coding sequence using primers F 3 (lower case: pCineo sequence; upper case: GatT coding sequence) and R 3 (lower case: pCineo sequence; upper case: GatT coding sequence).

Plasmid pCineo_mCherry_CAAX (encoding the plasma membrane marker mCherry_PM). The sequence encoding mCherry in frame with the polybasic sequence and CAAX motif of human K-Ras (GKKKKKKSKTKCVIM) for targeting to the plasma membrane was generated by amplification of mCherry using the pmCherry-N1 (Clontech) plasmid as template and the following primers: F 4 (lower case: pCineo sequence; upper case: mCherry coding sequence) and R 4 (lower case: pCineo sequence; italics: polybasic plus CAAX motif and stop codon coding sequence; upper case: mCherry coding sequence).

In vitro mRNA transcription and microinjections

Plasmids were linearized by digestion with NotI, a unique restriction site in the pCineo vector located downstream of the cloned sequences. One microgram of each linearized plasmid was used as template for *in vitro* transcription. Purified mRNAs were resuspended in DEPC-MilliQ water, their concentration measured, and their quality checked by agarose gel electrophoresis. mRNAs were aliquoted and stored at – 80°C until used.

Sea urchin eggs' jelly coat was dissolved by a short wash in acidic filtered sea water (1.5 mM citric acid in 0.22 μm filtered sea water, FSW). De-jellied eggs were then immobilized on 60 mm plastic dish lids pre-treated with 1% protamine sulfate (Merck, Sigma-Aldrich, P4380) in FSW. Eggs were then washed with FSW containing sodium para-amino benzoate (Sigma-Aldrich, A6928; 0.05% in FSW) to prevent hardening of the fertilization envelope. *In vitro* transcribed mRNAs were diluted to a final concentration of 300–500 ng/μL in 120 mM KCl/DEPC-water. Four to five pL of diluted mRNAs were injected per embryo, immediately after fertilization. Embryos were allowed to develop at 18°C.

Confocal microscopy

Paracentrotus lividus

At the indicated times post-fertilization, embryo development was stopped by incubation with 0.2% paraformaldehyde in FSW, which kills the embryos while preserving mEGFP and mCherry fluorescence. Imaging was carried out within 16 h of formaldehyde treatment. Embryos laid on glass-bottom dishes containing FSW were imaged with an inverted 25x (NA 0.8) water immersion objective, using a Zeiss LSM700 system. Image stacks (z-step 1 μm) were acquired. Only one-third to one-half of the embryo volumes could be imaged at early stages, due to the opacity of yolk granules. At later stages (prism and pluteus) embryos were transparent and their whole volume was imaged.

For live imaging experiments, eggs were laid in FWS containing glass-bottom dishes pre-treated with protamine, fertilized, and then immediately microinjected with fluorescent reporter encoding mRNAs. Imaging was carried out as described above. Image stacks (z-step 1 μm) were acquired at 15 min intervals. Higher magnification imaging of embryos was carried out on mEGFP_Giant-CT (mEGFP_Golgi) microinjected embryos using a 40x (NA 1.10) water immersion objective with a Leica SP8 confocal system. For presentation purposes only, contrast-enhancement and gaussian-blur filtering were carried out (ImageJ) for the images shown. *Human umbilical vein endothelial cells (HUVECs)*. Cells were seeded on gelatin-coated 96-well plates (Nunclon surface©, NUNC) at 15.000 cells/well and grown in HUVEC growth medium (HGM, see Ferraro et al.[101]) for 24 h. After rinsing with fresh medium, cells were fed HGM containing 0.1% (vol:vol) DMSO (control treatment) or 33 μM (10 mg/mL) Nocodazole and incubated for 4 h before fixation with 4% formaldehyde in phosphate-buffered saline (PBS) for 10 min at RT. Fixed cells were permeabilized with 0.2% TX-100 (Merck,

Please cite this article in press as: Benvenuto et al., Evolution of the ribbon-like organization of the Golgi apparatus in animal cells, Cell Reports (2024), https://doi.org/10.1016/j.celrep.2024.113791

Sigma-Aldrich) in PBS for 10 min (RT) and then blocked with 5% BSA (Merck, Sigma-Aldrich) in PBS for 30 min (RT). The Golgi apparatus was immuno-labeled with an antibody raised against the Golgi marker GM130 (BD Biosciences), followed by incubation with Alexa Fluor 488 conjugated anti-mouse antibody (Life Technologies); primary and secondary antibodies were diluted in 1% BSA/0.02% TX-100/PBS. Nuclei were counterstained with Hoechst 33342 (Life Technologies), diluted in PBS, and images acquired using an Opera High Content Screening System (PerkinElmer) through a 40× air objective (NA 0.6).

Golgi object quantification in sea urchin embryos

Golgi objects from confocal images were analyzed with ImageJ (https://imagej.nih.gov/ij/). The Golgi channel (8-bit) was selected, maximum intensity projection images generated and processed as follows.

Time course (Figures 3A and S4B). All images were subjected to background subtraction. Small Golgi objects observed at 2-, 4- and 6-h post-fertilization were identified with the "find maxima" command and separated from each other by segmentation. The images of all time points were then subjected to thresholding and transformed into binary images. Golgi object number and size were then quantified with the "analyze particles" command (area range was set at 0.25 – infinite μm^2). Three embryos per time point were analyzed. The number of Golgi objects analyzed were: 2527, 2 hpf; 2662, 4 hpf; 1131, 6 hpf; 614, 8 hpf; 620, 10 hpf.

Time-lapse (Figures 3B and 3C). Image thresholds were set automatically. At early time points, slight adjustments were done to correctly capture the size of most Golgi objects. For later time points, default threshold values were sufficient to correctly outline the size Golgi objects. After transformation into binary images, object number and size were measured as described above. The number of Golgi objects analyzed ranged from 86 to 590 and are reported as a plot in Figure 3C.

Numerical results were processed with Prism 9 (Graphpad) for graph plotting and statistical analysis.

Electron microscopy

Paracentrotus lividus, *Branchiostoma lanceolatum* and *Ciona robusta* samples, maintained at 18°C, were collected at the indicated developmental stages and fixed at 4°C in 2% glutaraldehyde in filtered sea water (FSW). After fixation samples were first rinsed in FSW (6 × 10 min), then in Milli-Q water (3 × 10 min) and post-fixed with 1% osmium tetroxide and 1.5% potassium ferrocyanide (1 h, 4°C). Samples were then rinsed five times with Milli-Q water, dehydrated in a graded ethanol series, further substituted by propylene oxide, and embedded in Epon 812 (TAAB Laboratories Equipment Ltd, Berkshire, UK). Resin blocks were sectioned with an Ultracut UCT ultramicrotome (Leica, Vienna, Austria). Sections were placed on nickel grids and observed with a Zeiss LEO 912AB TEM (Zeiss, Oberkochen, Germany).

Calloria inconspicua. Three-lobed larvae were initially fixed in 2.5% glutaraldehyde buffered with 0.1 M sodium cacodylate solution (60 min at 5°C). A tiny amount ruthenium red solution was added to stain the extracellular matrix. Repeated rinsing in 0.1 M sodium cacodylate buffer was followed by post-fixation in 1% osmium tetroxide solution buffered with 0.1 M sodium cacodylate (40 min at 4°C). Dehydration with an acetone series and propylene oxide led to embedding in Araldite. Resin blocks were polymerized at 60°C for 48 h. Ultrathin serial sections (70 nm) were cut on a Reichert Ultracut E microtome, placed on formvar-coated copper slot grids, and automatically stained with uranyl acetate and lead citrate in an LKB Ultrastainer. The sections were examined in Zeiss EM 10B and Zeiss EM 900 transmission electron microscopes.

Parhyale hawaiensis. Embryos were pre-fixed in 2.5% glutaraldehyde, 2% paraformaldehyde, 2% sucrose in sodium cacodylate buffer 0.1 M (SC buffer) overnight at 4°C. After several rinses in SC buffer at room temperature specimens were postfixed in 1% OsO4 in 0.1 M SC Buffer (2 h, room temperature), washed in SC buffer (1 h) and dehydrated in an ethanol series. Ethanol-preserved specimens were transferred to 100% acetone and propylene oxide and subsequently embedded in araldite. Ultrathin sections were cut on a Leica EM UC7, stained with Plano uranyl acetate replacement stain (UAR-EMS) and lead citrate and investigated in a LEO EM 906.

Strongylocentrotus purpuratus, *Platynereis dumerilii*, *Mnemiopsis leidyi*, *Oscarella carmela* and *Capsaspora owczarzaki* samples were high-pressure frozen, freeze substituted and processed as previously described.[41,99,102–104]

Trichoplax adhaerens. Animals, alive or pre-fixed, were high-pressure frozen/freeze substituted and embedded in Epon. Sections (70 nm) were cut with using a Leica Ultracut UCT ultramicrotome.

Symsagittifera roscoffensis. Animals were processed within three days of hatching. The head of a hatchling was processed by high-pressure freezing. Freeze substitution was carried out in a solution of 1% osmium tetroxide and 0.1% uranyl acetate in acetone. A Leica Ultracut UCT was used to generate 60–80 nm sections, which were poststained in a 2% uranyl acetate/lead citrate solution and transferred to formvar-coated slit grids. Sections were imaged with a Tecnai 12 Biotwin TEM, using a fast-scan F214A CCD camera controlled by the SerialEM software (Boulder Lab). Digital image stacks were imported into the TrakEM2 package.

Clytia hemisphaerica. Dissected tissue was high-pressure frozen with a Wohlwend Compact 03 high-pressure freezing machine (http://www.wohlwend-hpf.ch) using sea water as the freezing medium and then transferred to a frozen solution of 2% osmium in acetone under liquid nitrogen. The samples were freeze-substituted in a Leica AFS2 freeze-substitution machine (https://www.leica-microsystems.com). Samples were removed from the AFS chamber and allowed to reach room temperature. This was followed by 5 acetone washes for 5 min each. Samples were infiltrated with Polybed resin in a series of steps as follows: 1:3 resin to acetone overnight, 1:1 resin to acetone for 6 h, 3:1 resin to acetone overnight, 100% resin for 6 h followed by embedment in molds in fresh 100% resin and curation at 60°C for 2 days. Polymerized samples were then trimmed using an ultramicrotome to get their entire cross-section. Serial 60 nm sections were collected using an Automated Tape-Collecting Ultramicrotome, mapped, and imaged with a Zeiss Sigma FE-SEM as described previously.[105]

Please cite this article in press as: Benvenuto et al., Evolution of the ribbon-like organization of the Golgi apparatus in animal cells, Cell Reports (2024), https://doi.org/10.1016/j.celrep.2024.113791

Homology search

Canonical human GRASP (GRASP65 and GRASP55), Golgin-45 and GM130 amino acid sequences were used as initial queries. Homologs were searched in the target species using Basic Local Alignment Search Tool, BLAST, (BLASTp and TBLASTn) in available databases (Uniprot, NCBI, Ensembl). For specific target species, the search was carried out in dedicated databases.

Amphiura filiformis: http://www.echinonet.org.uk/blast/
Mnemiopsis leidyi: https://research.nhgri.nih.gov/mnemiopsis/sequenceserver/
Nematostella vectensis: http://marimba.obs-vlfr.fr/blast.
Unicellular holozoans: https://protists.ensembl.org.

Target genomes and, whenever available, transcriptomes were interrogated. Hits with the lowest E-value and highest query coverage were selected as candidate homologs and validated when by reverse BLAST on the human proteome the query was retrieved as the highest scoring. If this approach did not return a hit, homologs of evolutionarily closer species were used as queries. Golgin-45 homologs were not found in the choanoflagellates *Salpingoeca rosetta* and *Monosiga brevicollis*. To verify whether the gene loss was specific to these two species or a general feature of choanoflagellates, we searched available transcriptomes of several species[106]; no Golgin-45 was found in any of the species that were searched. Further validation of homology was obtained by subjecting the hits to sequence and structural analysis with InterProScan (https://www.ebi.ac.uk/interpro/search/sequence/) and by multiple sequence alignment with AliView and JalView to verify regions of sequence similarity.

Analysis of the C-terminal sequences of Golgin-45 and GM130 homologs

The PDZ binding motif and the cysteine pair are highly conserved in Golgin-45 homologs, with the exception of *Drosophila melanogaster*, whose cells lack ribbon-like Golgi organization, and in the single stack species *Trichoplax adhaerens* (refer to Figure S2F, Kondylis et al.,[24] Yano et al.,[25] and Figure 1H). Compared to the mammalian homologs, the spacing between the cysteine pair and the PDZ-binding motif is affected by extra or missing residues in *Caenorhabditis elegans*, *Hofstenia miamia*, *Mnemiopsis leidyi*, and in the single stack species *Amphimedon queenslandica*. Based on the X-ray structure (see Figure S2E), changes in the spacing between these two motifs can be expected to prevent binding of Golgin-45 to GRASP in these in the species. Overall, the presence and the correct spacing of the binding motifs in Golgin-45 homologs mirrors the presence of the ribbon-like structure in metazoans (see Figure 1K). With respect to GM130, the PDZ-binding motif and the stretch of hydrophobic amino acids necessary for interaction with GRASP65 are conserved in vertebrates, but not in other metazoans. Several non-vertebrate GM130 homologs display the presence of a cysteine pair (see Figure S2G), suggesting the possibility that GM130 and Golgin-45 originally bound to GRASP in a similar (Golgin-45-like) fashion. Evolution of the two vertebrate GRASP paralogs appears to have driven diversification of GM130 and Golgin-45 C-termini and binding conformations (see Figures S2E—S2G). Sequence analysis suggests that the structural features that mediate interaction in the mammalian GRASP/Golgin-45 complexes are generally conserved in the Golgin-45 homologs of extant species that display a ribbon-like organization and usually absent in those without this Golgi structure. With respect to GM130, the motifs required for GRASP65 binding are conserved only across the vertebrate homologs, whereas in other species a cysteine pair might be able to form an atypical zinc finger. It is plausible to conclude that the GM130 homologs of some metazoan species might be able to bind the conspecific GRASPs with a conformation similar to that of Golgin-45. Of note, in contrast to Golgin-45, GM130 homologs bearing the binding-permissive motifs do not mirror the presence of the ribbon-like Golgi organization, which may indicate that while both GM130 and Golgin-45 could have contributed to the stack tethering mechanism, GM130 later became dispensable. This possibility is supported by AlphaFold2 modeling. In non-vertebrate species where the ribbon-like Golgi organization is observed, AlphaFold2 predicts GRASP binding by Golgin-45 but not GM130 (refer to Figures 2D, S3I, and S3J).

Phylogenetic tree of chordate GRASPs

Chordate GRASP sequences (Datas S1A and S1B) were trimmed to the conserved GRASP domain and processed adopting the Maximum Likelihood method with IQ-TREE 2.[94] ModelFinder[95] was used to select the model of sequence evolution. The *Paracentrotus lividus* GRASP sequence was used as outgroup. The graphical file was generated using FigTree (http://tree.bio.ed.ac.uk/software/figtree/).

Structure modeling

Models of complexes between conspecific GRASP/Golgin-45 and GRASP/GM130 pairs were built with the Colab implementation of AlphaFold2,[71] using MMseqs2 to generate multiple sequences alignments.[107] To obtain reliable predictions of the protein-peptide complexes, AlphaFold-Multimer version v2 was used, with 12 recycles for the generation of each model.[74] Complexes were built without the use of structural templates and without Amber refinement as this step does not introduce substantial improvement, while significantly increasing computational time.

Interpretation and predictive power of AlphaFold2 models

The introduction of AlphaFold[70] and its subsequent evolutions produced a revolution in structural biology, allowing the generation of structure models of unprecedented accuracy. Benchmark studies have demonstrated that the predictive power of AF2 extends beyond the production of the mere structural models, yielding accurate results also for protein-protein and protein-peptide

Please cite this article in press as: Benvenuto et al., Evolution of the ribbon-like organization of the Golgi apparatus in animal cells, Cell Reports (2024), https://doi.org/10.1016/j.celrep.2024.113791

complexes, even when they imply conformational changes, and providing reliable hints on the effect of missense mutations.[108] In the case of protein-peptide complexes, models with higher confidence can be obtained by increasing the number of recycles during model generation, provided that a sufficient number of sequences are detected during the generation of the multiple sequence alignments (MSAs).[72,74] From these MSAs, AF2 predicts five structures resulting from five models trained according to different schemes.[70] These predictions are then evaluated and ranked based on a per residue score, the predicted local distance difference test (pLDDT). This value provides a measure, from a minimum of 0 to a maximum of 100, of the agreement between the prediction and experimental structures. Regions within proteins and complexes that present an average pLDDT $\geq$70 are generally considered reliable.[109] At the same time, it has been observed that low pLDDT values are indicative of intrinsically disordered regions and highly flexible stretches within proteins.[73,110] Therefore, stable complexes, in which the binding partners have reduced mobility with respect to each other, are typically modeled with higher pLDDT scores. We carried out validation tests on the predictive capability of AF2 on our model systems. To assess the results and the occurrence of binding, the highest-ranking structure from each AF2 prediction was used. Overall, similar confidence scores were obtained for each of the five independent models generated. High pLDDT scores and conformations very similar to the X-ray structures (PDB: 5H3J and 4REY, respectively) characterized the AF2 models of the mammalian GRASP55/Golgin-45 and GRASP65/GM130 complexes. Conversely, low pLDDT scores characterized complexes of the mutants of the Golgin-45 PDZ-binding motif and the cysteine pair, which were experimentally shown to abolish binding to GRASP55 (see Figures S4A and S4B).[67] The results were less straightforward for the mutants of GM130 that abolish binding to GRASP65,[68] for which the predictions still hinted to the possibility of forming complexes (see Figures S4C and S4D). However, it is worth noting that in the case of the inactivating I990R mutation in the PDZ-binding motif of human GM130, two lower ranking models predicted absence of binding. Most impressive was the test involving cross-binding. Biochemical data show that mammalian GRASP55 can interact with GM130, while GRASP65 does not bind GM130 (see Figures 1B and 1E of Short et al.[60]). AF2 modeled the GRASP55/GM130 complex with a high pLDDT score and a conformation similar to the GRASP65/GM130 complex, whereas the GRASP65/Golgin-45 complex was modeled with a low pLDDT score (see Figures S4E and S4F). Based on these tests, we considered AF2 models as indicative of binding when they displayed a conformation similar to that of the X-ray structure of the mammalian complexes and high pLDDT score for the motifs necessary to binding. Based on these criteria, we built models for representative GRASP/Golgin-45 and GRASP/GM130 pairs from different species; the GRASPs from all species were modeled with overall high confidence (average pLDDT $\geq$90), whereas variable results were obtained for the C-terminal peptides of the Golgin-45 and GM130 proteins. In particular, C-termini lacking the PDZ-binding motif and/or the cysteines for Zn-finger formation (e.g., *Drosophila melanogaster* and *Trichoplax adhaerens*) could not adopt the Golgin-45 binding conformation and were associated to very low pLDDT values. Of note, the Golgin-45 C terminus of *Parhyale hawaiensis* presents both binding motifs with the same spacing as that seen in the vertebrate homologs (see Figure S2F). This suggests that the GRASP/Golgin-45 complex could form in this species that displays separated Golgi stacks (see Figure 1E). However, AF2 modeled the region encompassing the cysteine pair with a pLDDT score <70, thus predicting absence of binding (data not shown). As for GM130, in non-vertebrates, the pLDDT were generally low. Strikingly, as anticipated by the amino acid sequence analysis, the presence of cysteine pairs resulted in the prediction of a Golgin-45-like conformation in *T. adhaerens* and *A. queenslandinca*, suggesting that the ancestral GM130 protein could bind GRASP even in animals with a single stack per cell. Although Golgin-45-like conformations were observed in the predicted complexes of other species, the region containing the cysteine pair was modeled with low pLDDT scores and therefore were, conservatively, considered as not interacting.

Note about Figure 2A. Golgin and GRASP localization within the stack and their evolutionary emergence were obtained from references[44,45,69] and [111].

Note about the metazoan Tree of Life. Whether sponges or ctenophores or placozoans are the sister group to all other animals remains an unsettled issue[112–114]; for this reason we drew the holozoan Tree of Life as a polytomy of these three taxa in Figures 1K and 2E and in the graphical abstract. The animal silhouettes used in the graphical abstract were obtained from the public domain (http://phylopic.org), when not covered by copyright, or drawn by F.F.

QUANTIFICATION AND STATISTICAL ANALYSIS

Statistical analysis of the number of Golgi objects was carried out using the Mann-Whitney test; p values are indicated in the legends of Figures 3 and S4. The number of objects per time point analyzed is reported in the "Golgi object quantification in sea urchin embryos" section of the "method details".

Cell Reports, Volume ■ ■

Supplemental information

Evolution of the ribbon-like organization of the Golgi apparatus in animal cells

Giovanna Benvenuto, Serena Leone, Emanuele Astoricchio, Sophia Bormke, Sanja Jasek, Enrico D'Aniello, Maike Kittelmann, Kent McDonald, Volker Hartenstein, Valentina Baena, Héctor Escrivà, Stephanie Bertrand, Bernd Schierwater, Pawel Burkhardt, Iñaki Ruiz-Trillo, Gáspár Jékely, Jack Ullrich-Lüter, Carsten Lüter, Salvatore D'Aniello, Maria Ina Arnone, and Francesco Ferraro

Figure S1

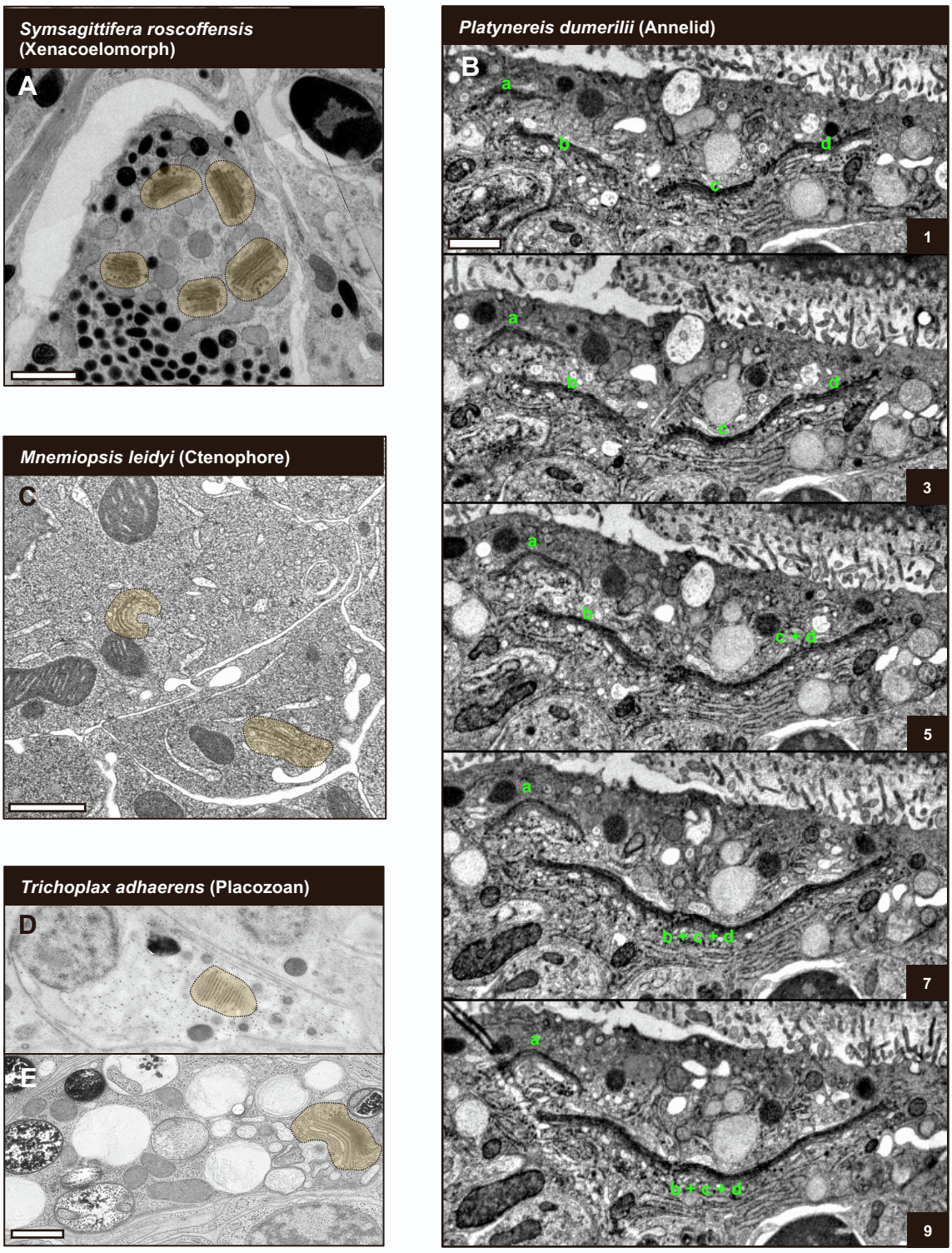

F

Species	Taxon	Multiple Golgi stacks per cell	Presence of ribbon-like Golgi	Source of morphological data	Tissues/cell types
C. robusta	Tunicates	+	+	This paper	epidermal cells of larva
B. lanceolatum	Cephalocordates	+	+	This paper	ectodermal cells of gastrula
S. purpuratus	Echinoderms	+	+	This paper	blastocoelar cells of pluteus larva
P. lividus	Echinoderms	+	+	This paper	all cells from pre-hatching blastula to pluteus larva
L. variegatus	Echinoderms	+	+	Literature	all cells in pre-hatching blastula
L. pictus	Echinoderms	+	+	Literature	all cells in blastula and prism stage
D. melanogaster	Arthropods	+	–	Literature	all cell types (larva and adult) and cell lines
A. mellifera	Arthropods	+	–	Literature	Trophocyte
A. pisum	Arthropods	+	–	Literature	Mycetocytes
A. albopictus	Arthropods	+	–	Literature	cell line
P. hawaiensis	Arthropods	+	–	This paper	all cell types (adult)
C. elegans	nematodes	+	–	Literature	all cell types
C. inconspicua	Brachiopods	+	–	This paper	epidermal cells of 3-lobe larva
P. vivipara	Mollusks	+	+	Literature	spermatocytes
H. pomatia	Mollusks	+	+	Literature	multified gland cells
H. aspersa	Mollusks	+	+	Literature	early spermatocytes
P. dumerilii	Annelids	+	+	This paper	several cell types of 3-day-old larva
Lumbricus (unreported species)	Annelids	+	+	Literature	epithelial cells and neurons of adult
S. roscoffensis	Xenacoelomorphs	+	+	This paper	secretory granule producing cells
C. hemisphaerica	Cnidarians	+	+	This paper	gastrodermal cells of adult
M. leidyi	Ctenophores	+	–	This paper	epithelial and comb cells
T. adhaerens	Placozoans	–	N/A	This paper	all cell types
H. hongkongensis	Placozoans	–	N/A	Literature	all cell types
O. carmela	Sponges	–	N/A	Literature and this paper	all cell types
E. fluviatilis	Sponges	+	–	Literature	spongocyte
S. rosetta	Choanoflagellates	–	N/A	Literature	N/A
C. owczarzaki	Filastereans	–	N/A	This paper	N/A

Figure S1. Additional examples of Golgi structure in holozoans. Related to Figure 1. (A) Golgi stack array in secretory cells of *Symsagittifera roscoffensis*. (B) A three-day-old *Platynereis dumerilii* larva. Serial sections (40 nm each), labelled starting from 1, are shown; in the region of interest, separated stacks (labelled a, b, c and d) in section 1 are seen to merge (c + d and then b + c + d) into a ribbon while progressing through the sections. (C) Comb cells of *Mnemiopsis leidyi*. (D-E) Two cell types of *Trichoplax adhaerens*. Scale bars: 1 μm. (F) Table summarizing Golgi organization in species and cell types discussed in this report.

Figure S2

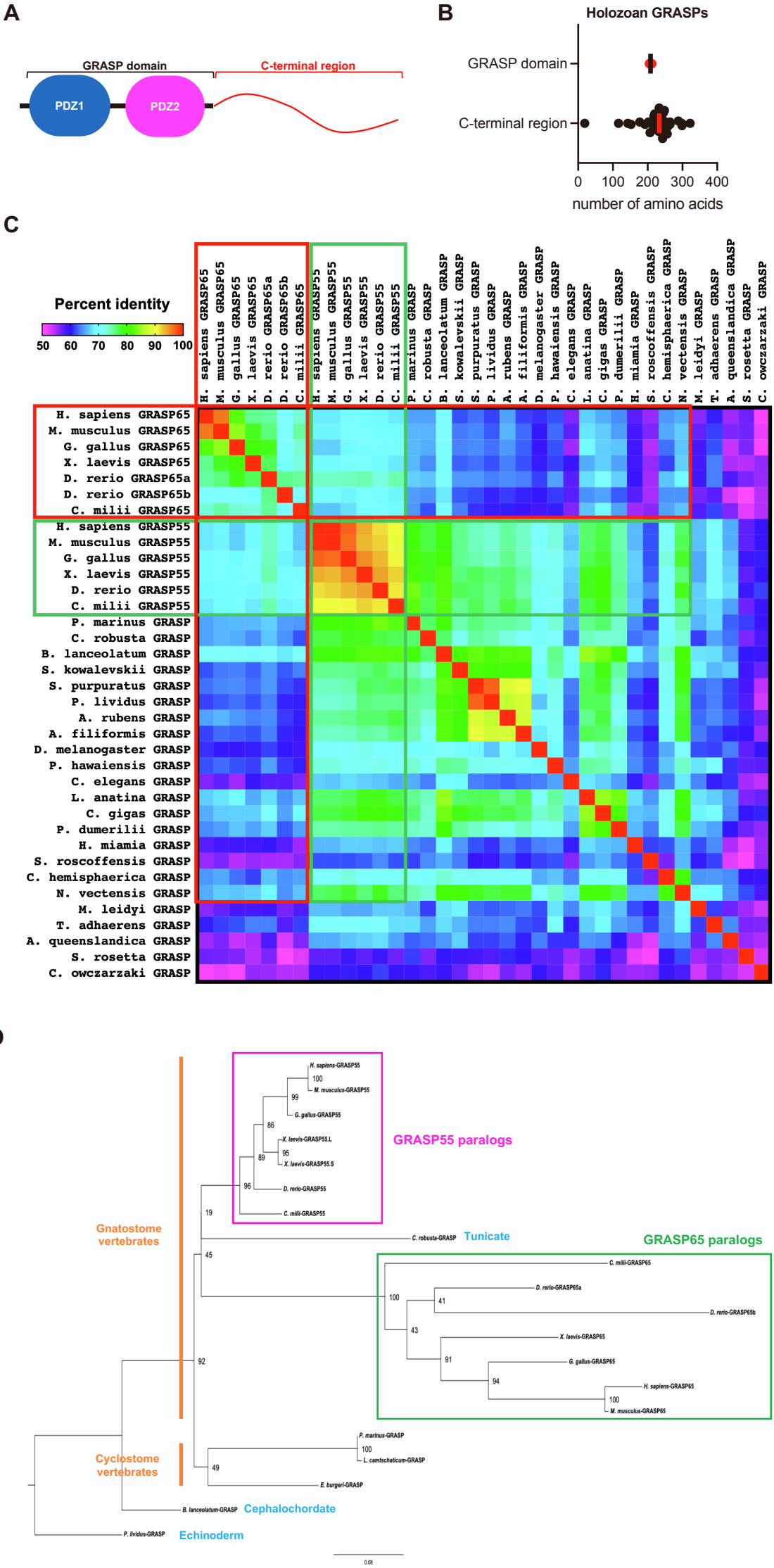
A
GRASP domain
C-terminal region
PDZ1
PDZ2
B
Holozoan GRASPs
GRASP domain
C-terminal region
0
100
200
300
400
number of amino acids
C
Percent identity
50
60
70
80
90
100
H. sapiens GRASP65
M. musculus GRASP65
G. gallus GRASP65
X. laevis GRASP65
D. rerio GRASP65a
D. rerio GRASP65b
C. milii GRASP65
H. sapiens GRASP55
M. musculus GRASP55
G. gallus GRASP55
X. laevis GRASP55
D. rerio GRASP55
C. milii GRASP55
P. marinus GRASP
C. robusta GRASP
B. lanceolatum GRASP
S. kowalevskii GRASP
S. purpuratus GRASP
P. lividus GRASP
A. rubens GRASP
A. filiformis GRASP
D. melanogaster GRASP
P. hawaiensis GRASP
C. elegans GRASP
L. anatina GRASP
C. gigas GRASP
P. dumerilii GRASP
H. miamia GRASP
S. roscoffensis GRASP
C. hemisphaerica GRASP
N. vectensis GRASP
M. leidyi GRASP
T. adhaerens GRASP
A. queenslandica GRASP
S. rosetta GRASP
C. owczarzaki GRASP
D
GRASP55 paralogs
GRASP65 paralogs
Gnatostome vertebrates
Cyclostome vertebrates
Tunicate
Cephalochordate
Echinoderm
H. sapiens-GRASP55
M. musculus-GRASP55
G. gallus-GRASP55
X. laevis-GRASP55.L
X. laevis-GRASP55.S
D. rerio-GRASP55
C. milii-GRASP55
C. robusta-GRASP
C. milii-GRASP65
D. rerio-GRASP65a
D. rerio-GRASP65b
X. laevis-GRASP65
G. gallus-GRASP65
H. sapiens-GRASP65
M. musculus-GRASP65
P. marinus-GRASP
L. camtschaticum-GRASP
E. burgeri-GRASP
B. lanceolatum-GRASP
P. lividus-GRASP
0.08

E

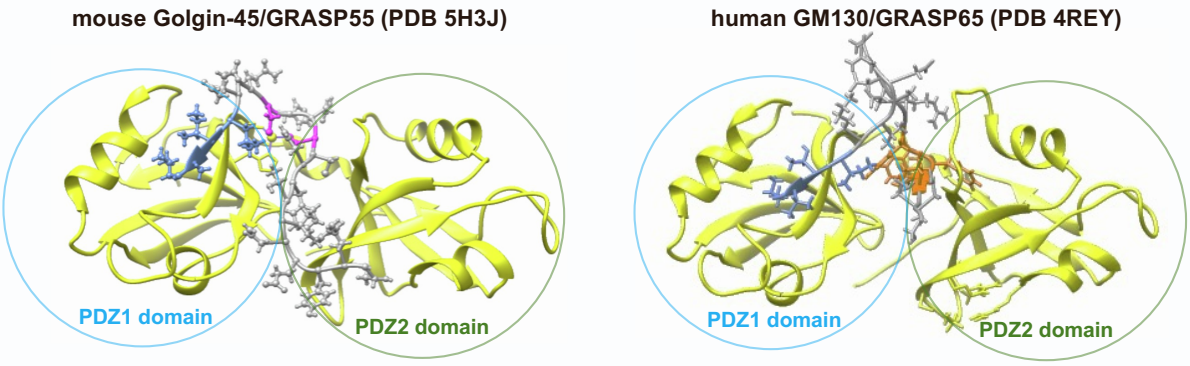
mouse Golgin-45/GRASP55 (PDB 5H3J)
PDZ1 domain
PDZ2 domain
human GM130/GRASP65 (PDB 4REY)
PDZ1 domain
PDZ2 domain

F

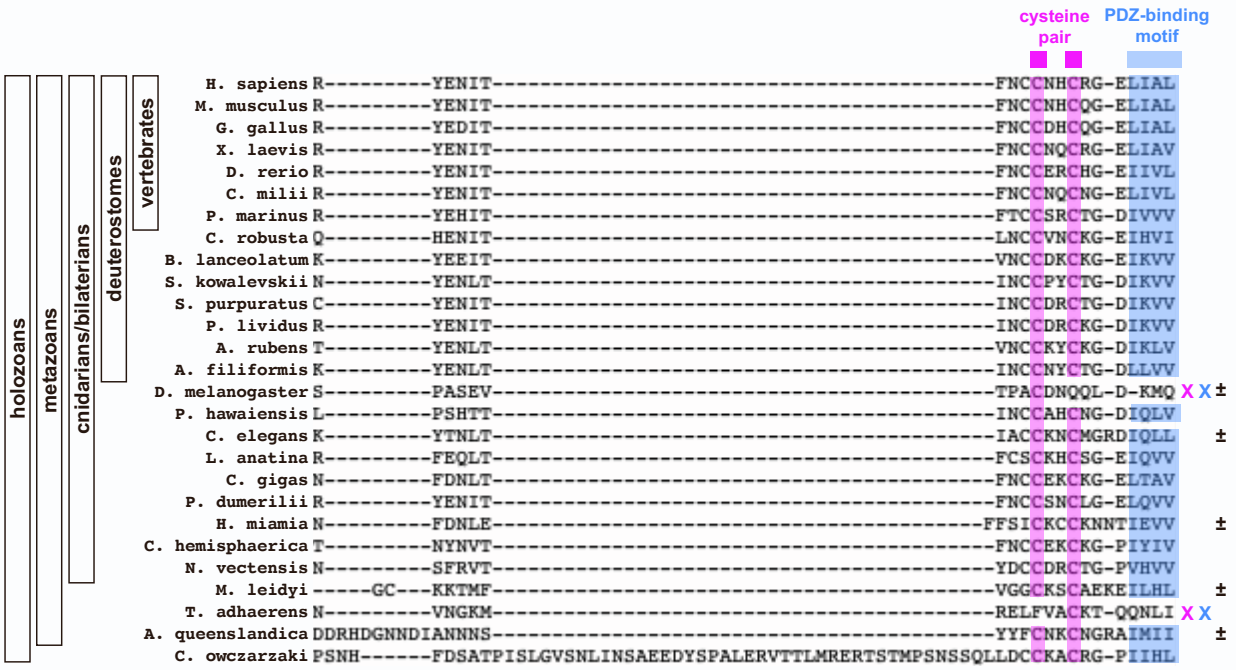
cysteine pair
PDZ-binding motif
holozoans
metazoans
cnidarians/bilaterians
deuterostomes
vertebrates
H. sapiens R---------YENIT----------FNCCNHCRG-ELIAL
M. musculus R---------YENIT----------FNCCNHCQG-ELIAL
G. gallus R---------YEDIT----------FNCCDHCQG-ELIAL
X. laevis R---------YENIT----------FNCCNQCRG-ELIAV
D. rerio R---------YENIT----------FNCCERCHG-EIIVL
C. milii R---------YENIT----------FNCCNQCNG-ELIVL
P. marinus R---------YEHIT----------FTCCSRCTG-DIVVV
C. robusta Q---------HENIT----------LNCCVNCKG-EIHVI
B. lanceolatum K---------YEEIT----------VNCCDKCKG-EIKVV
S. kowalevskii N---------YENLT----------INCCPYCTG-DIKVV
S. purpuratus C---------YENIT----------INCCDRCTG-DIKVV
P. lividus R---------YENIT----------INCCDRCKG-DIKVV
A. rubens T---------YENLT----------VNCCKYCKG-DIKLV
A. filiformis K---------YENLT----------INCCNYCTG-DLLVV
D. melanogaster S---------PASEV----------TPACDNQQL-D-KMQ X X ±
P. hawaiensis L---------PSHTT----------INCCAHCNG-DIQLV
C. elegans K---------YTNLT----------IACCKNCMGRDIQLL ±
L. anatina R---------FEQLT----------FCSCKHCSG-EIQVV
C. gigas N---------FDNLT----------FNCCEKCKG-ELTAV
P. dumerilii R---------YENIT----------FNCCSNCLG-ELQVV
H. miamia N---------FDNLE----------FFSICKCCKNNTIEVV ±
C. hemisphaerica T---------NYNVT----------FNCCEKCKG-PIYIV
N. vectensis N---------SFRVT----------YDCCDRCTG-PVHVV
M. leidyi -----GC---KKTMF----------VGGCKSCAEKEILHL ±
T. adhaerens N---------VNGKM----------RELFVACKT-QQNLI X X
A. queenslandica DDRHDGNNDIANNNS----------YYFCNKCNGRAIMII ±
C. owczarzaki PSNH------FDSATPISLGVSNLINSAEEDYSPALERVTTLMRERTSTMPSNSSQLLDCCKACRG-PIIHL

G

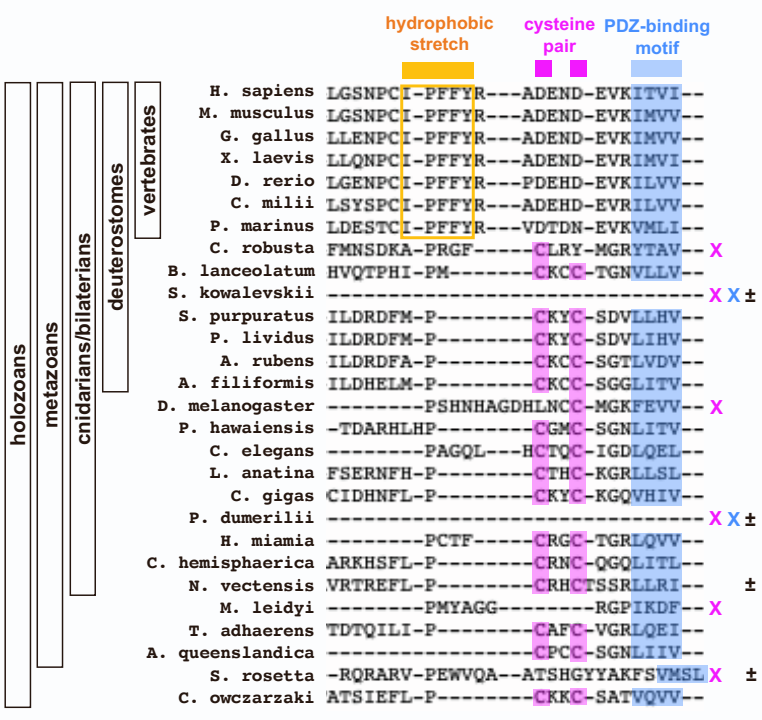
hydrophobic stretch
cysteine pair
PDZ-binding motif
holozoans
metazoans
cnidarians/bilaterians
deuterostomes
vertebrates
H. sapiens LGSNPCI-PFFYR---ADEND-EVKITVI--
M. musculus LGSNPCI-PFFYR---ADEND-EVKIMVV--
G. gallus LLENPCI-PFFYR---ADEND-EVKIMVV--
X. laevis LLQNPCI-PFFYR---ADEND-EVRIMVI--
D. rerio LGENPCI-PFFYR---PDEHD-EVKILVV--
C. milii LSYSPCI-PFFYR---ADEHD-EVRILVV--
P. marinus LDESTCI-PFFYR---VDTDN-EVKVMLI--
C. robusta FMNSDKA-PRGF-----CLRY-MGRYTAV-- X
B. lanceolatum HVQTPHI-PM-------CKCC-TGNVLLV--
S. kowalevskii ---------- X X ±
S. purpuratus ILDRDFM-P---------CKYC-SDVLLHV--
P. lividus ILDRDFM-P---------CKYC-SDVLIHV--
A. rubens ILDRDFA-P---------CKCC-SGTLVDV--
A. filiformis ILDHELM-P---------CKCC-SGGLITV--
D. melanogaster --------PSHNHAGDHLNCC-MGKFEVV-- X
P. hawaiensis -TDARHLHP---------CGMC-SGNLITV--
C. elegans --------PAGQL---HCTQC-IGDLQEL--
L. anatina FSERNFH-P---------CTHC-KGRLLSL--
C. gigas CIDHNFL-P---------CKYC-KGQVHIV--
P. dumerilii ---------- X X ±
H. miamia --------PCTF-----CRGC-TGRLQVV--
C. hemisphaerica ARKHSFL-P---------CRNC-QGQLITL--
N. vectensis VRTREFL-P---------CRHCTSSRLLRI-- ±
M. leidyi --------PMYAGG---------RGPIKDF-- X
T. adhaerens TDTQILI-P---------CAFC-VGRLQEI--
A. queenslandica ---------- CPCC-SGNLIIV--
S. rosetta -RQRARV-PEWVQA--ATSHGYYAKFSVMSL X ±
C. owczarzaki ATSIEFL-P---------CKKC-SATVQVV--

Figure S2. Structural features of holozoan GRASP and Golgin-45 proteins. Related to Figure 2. (A) Cartoon of domain structure of mammalian GRASPs. The evolutionarily conserved GRASP domain is formed by a tandem of atypical PDZ domains, followed by a C-terminal region, which in mammals is serine/proline-rich (SPR) and whose post-translational modifications modulate GRASP activity. (B) Size, in amino acids, of the GRASP domains and C-terminal regions of the holozoan GRASP sequences (Data S1A) were plotted; bars indicate median size. (C) Pairwise amino acid identity of holozoan GRASP domains plotted as a heat map. Vertebrate duplication into GRASP55 and GRASP65 paralogs occurred with the evolution of jawed vertebrates. Vertebrate GRASP55 paralogs (green outlines) are more similar to the cnidarian/bilaterian single GRASPs than vertebrate GRASP65 paralogs (red outlines); percent identity values for pairwise comparisons were obtained with CLUSTAL omega. (D) Phylogenetic tree of chordate GRASPs. Divergence from the ancestor sequence is lower in GRASP55 paralogs when compared to GRASP65 ones; the *Paracentrotus lividus* sequence was used as outgroup. Note that for the fast-evolving species *Ciona robusta* the position of its single GRASP homolog does not reflect the tree of life. The numbers indicate bootstrap values; the scale indicates the average amino acid substitution per site. (E) X-ray structures of the GRASPs domains (yellow) of GRASP55 and GRASP65 in complex, respectively, with the C-terminal residues of Golgin-45 and GM130 (ball and stick); PDB accession numbers of the two complexes are indicated. PDZ1 and PDZ2 are indicated by circles. C-terminal residues experimentally shown to be necessary for interaction are rendered in color. Golgin-45: magenta, the two cysteines involved in the Zinc-like finger formation; light blue, the PDZ-binding motif. GM130: orange, the hydrophobic stretch interacting with the groove between the PDZ1 and PDZ2 domains; light blue, the PDZ-binding motif. (F) Multiple sequence alignment of the C-termini of the holozoan Golgin-45 homologs. The residues corresponding to the binding motifs are color coded as in Figure S2E. Insertions and deletions with respect to the mouse sequence are indicated by the symbol ±; mutations affecting the PDZ-binding motif and the cysteine pair are indicated by the blue and magenta symbol X, respectively. (G) Multiple sequence alignment of the C-termini of the holozoan GM130 homologs. The residues corresponding to the binding features of vertebrate homologs are color coded as in Figure S2E. In non-vertebrate homologs a cysteine pair, similar to that present in Golgin-45, is observed

in several proteins (labelled in magenta as in S2F). Mutations in the binding motifs and indels are indicated as described in S2F.

Figure S3

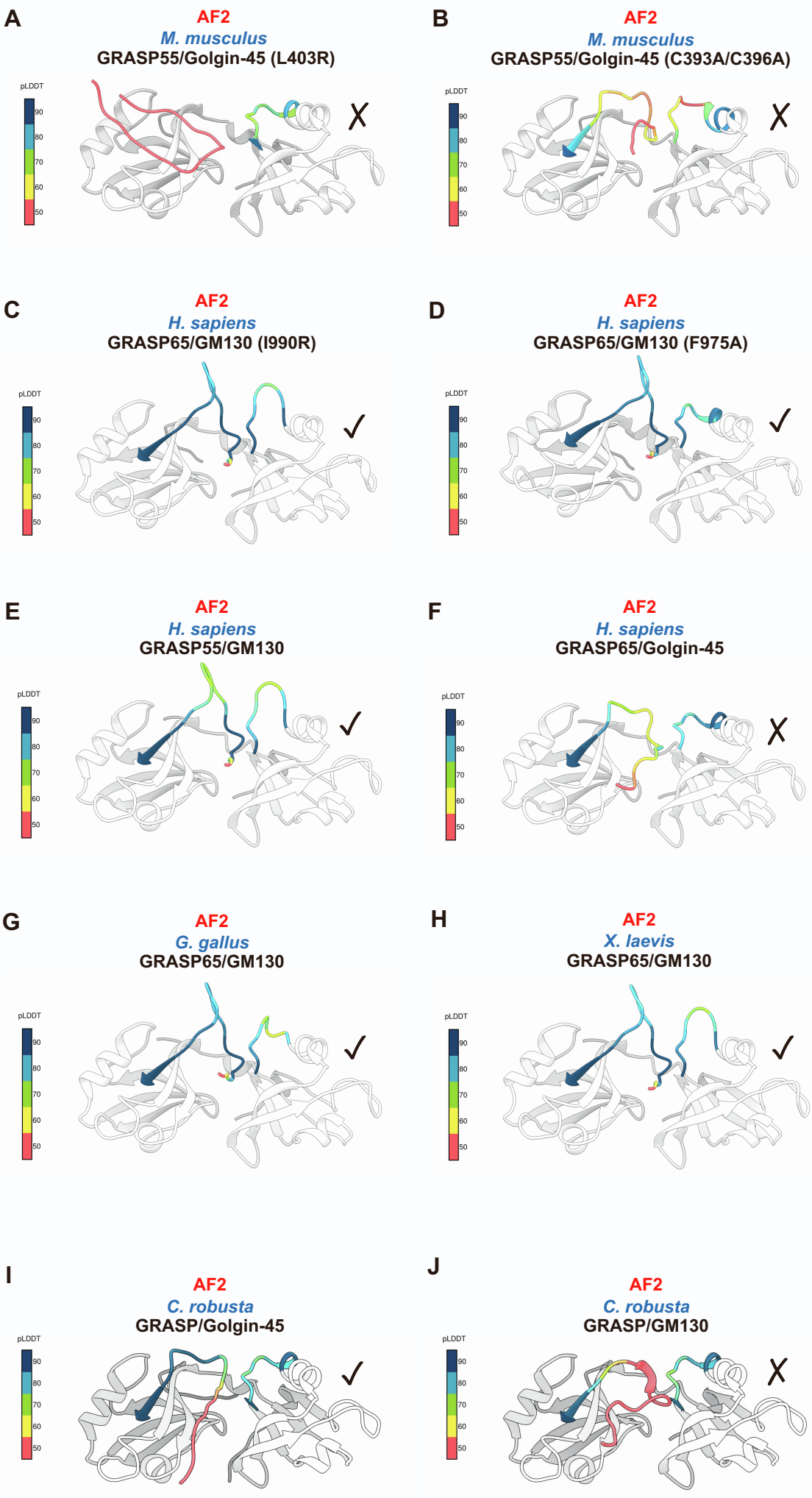
A
AF2
M. musculus
GRASP55/Golgin-45 (L403R)
pLDDT
90
80
70
60
50
X
B
AF2
M. musculus
GRASP55/Golgin-45 (C393A/C396A)
pLDDT
90
80
70
60
50
X
C
AF2
H. sapiens
GRASP65/GM130 (I990R)
pLDDT
90
80
70
60
50
✓
D
AF2
H. sapiens
GRASP65/GM130 (F975A)
pLDDT
90
80
70
60
50
✓
E
AF2
H. sapiens
GRASP55/GM130
pLDDT
90
80
70
60
50
✓
F
AF2
H. sapiens
GRASP65/Golgin-45
pLDDT
90
80
70
60
50
X
G
AF2
G. gallus
GRASP65/GM130
pLDDT
90
80
70
60
50
✓
H
AF2
X. laevis
GRASP65/GM130
pLDDT
90
80
70
60
50
✓
I
AF2
C. robusta
GRASP/Golgin-45
pLDDT
90
80
70
60
50
✓
J
AF2
C. robusta
GRASP/GM130
pLDDT
90
80
70
60
50
X

Figure S3. Testing AlphaFold2 model predictions. Related to Figure 2. (A)-(D) Models of GRASP domains of mammalian GRASP55 and GRASP65 with the C-termini of Golgin-45 and GM130 bearing mutations that were shown to abolish interaction. (E) Model of the GRASP domain of human GRASP55 and the GM130 C-terminus; a conformation similar to the GRASP65/GM130 complex is predicted. (F) Model of the GRASP domain of human GRASP65 and the Golgin-45 C-terminus. (G)-(H) AF2 predicts vertebrate GRASP65/GM130 complexes with conformations similar to the human solved structure; the chicken (*Gallus gallus*) and the African clawed frog (*Xenopus laevis*) complexes are shown. (H)-(I) Models of the complexes of *C. robusta* GRASP with the conspecific Golgin-45 and GM130 C-termini. Based on these tests, AF2 seems to predict binding when two conditions are met: a conformation similar to that of the X-ray structure and a reliable pLDDT score (≥ 70) within the golgins' motifs crucial for interaction. As in Figure 2D, the symbols ✓ and ✗ respectively indicate deduced presence and absence of interaction between GRASP domains and the golgins' C-termini.

Figure S4

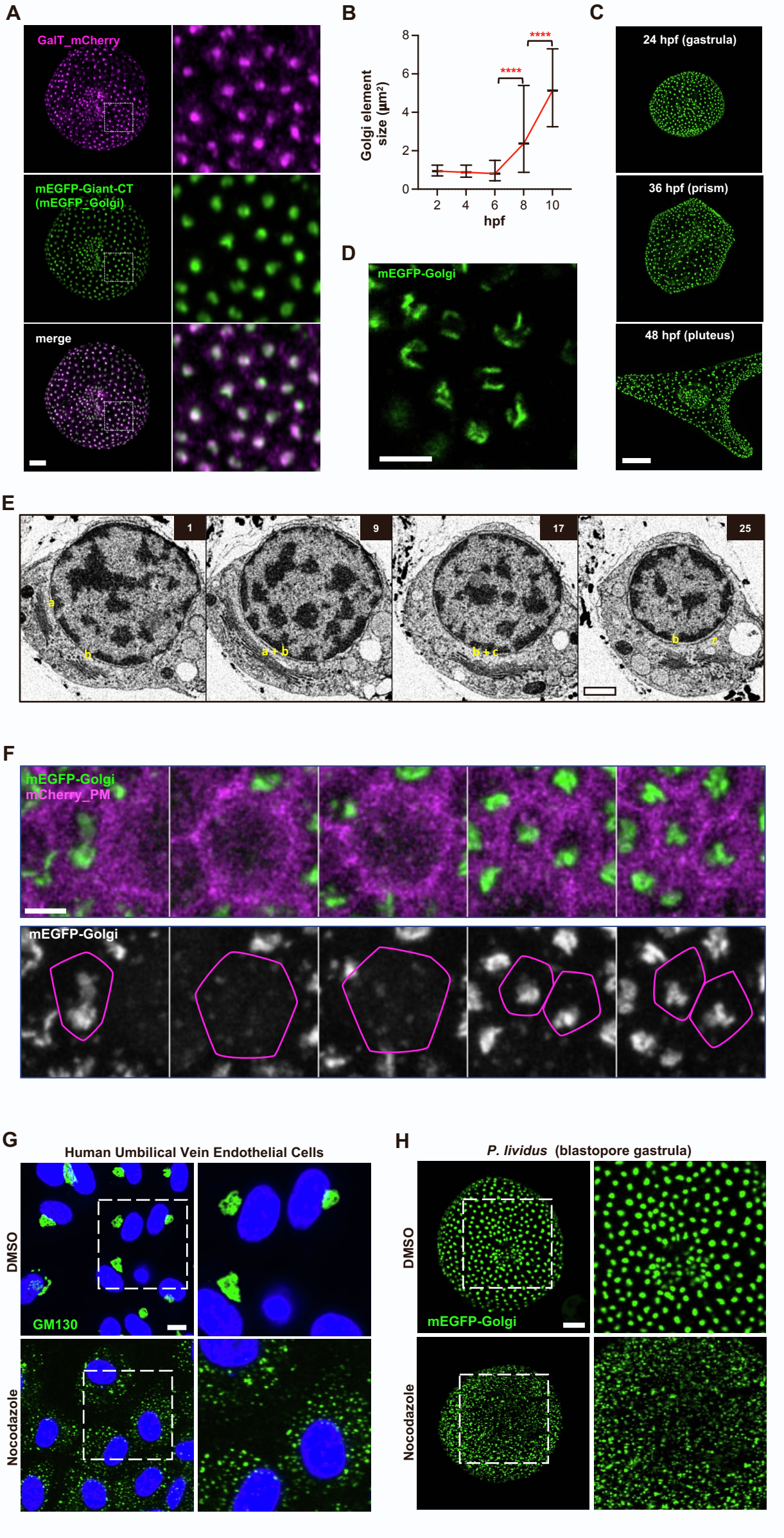
A
GalT_mCherry
mEGFP-Giant-CT
(mEGFP_Golgi)
merge
B
Golgi element size (µm²)
hpf
****
****
C
24 hpf (gastrula)
36 hpf (prism)
48 hpf (pluteus)
D
mEGFP-Golgi
E
1
9
17
25
a
b
a + b
b + c
c
F
mEGFP-Golgi
mCherry_PM
mEGFP-Golgi
G
Human Umbilical Vein Endothelial Cells
DMSO
Nocodazole
GM130
H
P. lividus (blastopore gastrula)
DMSO
Nocodazole
mEGFP-Golgi

Figure S4. Golgi dynamics in the sea urchin embryo. Related to Figure 3. (A) The fluorescent reporter used in this study, mEGFP_Golgi, co-localizes with the widely used Golgi reporter GalT_mCherry in the sea urchin (*Paracentrotus lividus*) early gastrula; scale bar: 20 µm. (B) Quantification of Golgi object size (n = 3 embryos) from the time-course experiment shown in Figure 1A; ****, $p < 0.0001$ (Mann-Whitney test). (C) *P. lividus* embryos expressing the mEGFP_Golgi reporter imaged at the indicated stages; scale bar: 50 µm. (D) Golgi apparatus imaging of a 15 hpf *P. lividus* embryo. A single focal plane acquired with a 40x water immersion objective is shown; scale bar: 5 µm. (E) Golgi stacks a, b and c are seen establishing connections across serial sections (numbered in black), of a blastocoel cell of the sea urchin *Strongylocentrotus purpuratus* pluteus; scale bar: 1 µm. (F) Golgi disassembly/reassembly during mitosis in the *P. lividus* embryo; image series (left to right, 15 min acquisition interval); scale bar: 5 µm. (G-H) Treatment with the microtubule depolymerizing compound nocodazole induces ribbon unlinking into constituent Golgi stacks in human umbilical vein endothelial cells, HUVECs, and sea urchin embryos; magnifications of insets are shown; scale bars: 10 µm and 20 µm (HUVECs and sea urchin, respectively).